Effects of antecedent hydrologic conditions, time dependence, and climate cycles on the suspended sediment load of the Salinas River, California

Citation	Gray, A. B., Pasternack, G. B., Watson, E. B., Warrick, J. A., & Goñi, M. A. (2015). Effects of antecedent hydrologic conditions, time dependence, and climate cycles on the suspended sediment load of the Salinas River, California. Journal of Hydrology, 525, 632-649. doi:10.1016/j.jhydrol.2015.04.025
DOI	10.1016/j.jhydrol.2015.04.025
Publisher	Elsevier
Version	Version of Record
Terms of Use	http://cdss.library.oregonstate.edu/sa-termsofuse

Journal of Hydrology 525 (2015) 632–649

Contents lists available at ScienceDirect

Journal of Hydrology

journal homepage: www.elsevier.com/locate/jhydrol

Effects of antecedent hydrologic conditions, time dependence, and climate cycles on the suspended sediment load of the Salinas River, California

Andrew B. Gray [a,*], Gregory B. Pasternack [a], Elizabeth B. Watson [a,1], Jonathan A. Warrick [b], Miguel A. Goñi [c]

[a] Department of Land, Air and Water Resources, University of California, 1 Shields Ave., Davis, CA 95616, USA
[b] U.S. Geological Survey, Pacific Coastal and Marine Science Center, 400 Natural Bridges Dr., Santa Cruz, CA 95060, USA
[c] College of Earth, Ocean and Atmospheric Sciences, 104 CEOAS Administration Bldg., Oregon State University, Corvallis, OR 97331-5503, USA

ARTICLE INFO

Article history:
Received 30 January 2014
Received in revised form 11 April 2015
Accepted 13 April 2015
Available online 20 April 2015
This manuscript was handled by Andras Bardossy, Editor-in-Chief, with the assistance of Alin Andrei Carsteanu, Associate Editor

Keywords:
Suspended sediment
Non-stationary
Effective discharge
El Niño Southern Oscillation
Small mountainous rivers
Arid rivers

SUMMARY

Previous estimations of sediment flux for the Salinas River of central California were based on data collected in the 1970s and assumptions of time invariant suspended sediment–discharge behavior. The goals of this study were to estimate sediment flux from the Salinas River using data from 1967–2011 by incorporating time dependent behavior and reassess the role of El Niño Southern Oscillation patterns in inter-decadal sediment load. This study builds on previous findings that time-dependent suspended sediment behavior in this system is controlled in part by antecedent hydrologic conditions. The condition of temporal dependence was further tested herein through comparison of flux estimates obtained using time-dependent formulations and a multivariate approach incorporating hydrologic factors. Longer sampling records and incorporation of decadal scale behavior or antecedent hydrologic conditions resulted in average annual load estimates of 2.0–2.9 Mt/yr with 95% confidence intervals of ±25 to 202%, in comparison to earlier estimates of ~3.3 Mt/yr. Previous overestimation of sediment load is due largely to the extrapolation of suspended sediment behavior from a decade of high sediment concentrations to the entire record, and the use of log-linear regression techniques on a non-linear system. The use of LOESS methods lowered Q_{SS} estimates and decreased confidence interval size. The inclusion of time-stratified and antecedent flow indices further decreased Q_{SS} estimates, but increased confidence interval size. However, temporal dependence of the C_{SS}–Q relationship violates the assumptions of single base period regression, which suggests that time-stratified rating curves provide more realistic estimates of sediment flux means and uncertainty. The majority of suspended sediment was transported by flows of ~25–90 times mean discharge depending on transport constituent (fines or sand) and estimation method. Periods of differential suspended sediment behavior changed the relative importance of rare floods due to changes in the relationship of suspended sediment concentration vs. discharge. El Niño years dominated the sediment budget by producing on average ten times more sediment than non-El Niño years. Sediment load estimates provided further evidence that antecedent hydrologic conditions appear to have caused much of the temporal dependence of suspended sediment behavior.

1. Introduction

Most of the mass flux from terrestrial to oceanic spheres occurs as suspended river sediment, and most suspended sediment is transported by small (~10 to 10^4 km^2 catchment area), high relief rivers (Milliman and Syvitski, 1992). Such rivers are often prone to highly episodic sediment load behavior due to highly variable hydrologic regimes and nonlinear relationships between the supplies of sediment and water to the channel. These suspended sediment concentration (C_{SS})–discharge (Q) 'rating' relationships can also change over time due to changes in the conditions moderating sediment and/or water supply. Thus, accurate, multi-decadal estimates of suspended sediment flux from small rivers are complicated by highly variable behavior over time, the dynamics of which are often poorly described due to a lack of field data.

* Corresponding author. Tel.: +1 530 752 1130.
E-mail addresses: abgray@ucdavis.edu (A.B. Gray), gpast@ucdavis.edu (G.B. Pasternack), elizabeth.b.watson@drexel.edu (E.B. Watson), jwarrick@usgs.gov (J.A. Warrick), mgoni@coas.oregonstate.edu (M.A. Goñi).
[1] Current address: Department of Biodiversity, Earth and Environmental Science, Academy of Natural Sciences of Drexel University, Philadelphia, PA 19103, USA.

http://dx.doi.org/10.1016/j.jhydrol.2015.04.025
0022-1694/

It has long been recognized that suspended sediment behavior can be dependent on antecedent conditions across a broad domain of temporal scales. Hysteresis, or path dependence, is the most common event scale phenomenon in suspended sediment behavior, whereby different C_{SS}–Q relationships are observed for the rising and subsequent falling limbs of a given event hydrograph (Williams, 1989). Seasonal effects are also commonly considered, particularly in areas that experience cold winters with prolonged frozen conditions or areas with monsoonal precipitation regimes that may experience sediment exhaustion as the rainy season progresses (e.g. Walling, 1977). More recent studies have also incorporated temporal dependence in suspended sediment rating curves. Interannual to inter-decadal patterns of sediment behavior due to the effects of large flooding events (Kelsey, 1980; Klein and Anderson, 2012; Warrick et al., 2013), wildfire (Shakesby and Doerr, 2006; Warrick et al., 2012) urbanization (Warrick and Rubin, 2007) and combined land use changes (Pasternack et al., 2001) have all been shown to significantly affect decadal to inter-decadal scale suspended sediment flux.

Suspended sediment load is the product of C_{SS} and Q over time. Thus the concentration of any given transported constituent (e.g., any grain size fraction) together with the frequency distribution of discharge can be used to understand which flows are most significant for transporting that constituent. Effective discharge $Q(e)$, a concept coined by Wolman and Miller (1960), is the magnitude of discharge that produces the most of a given transported constituent over a given period. Effective discharge has been a measure of great interest in a wide range of environmental research including those concerned with fluvial geomorphic control (Andrews, 1980; Webb and Walling, 1982), terrestrial organic carbon flux to the oceans (Wheatcroft et al., 2010) and suspended sediment load behavior (Nash, 1994; Gao et al., 2007). Another useful method for examining discharge frequency control on water and water-transported constituents is the 'half-load discharge' ($Q_{1/2}$) (Vogel et al., 2003). Whereas $Q(e)$ is the estimation of the discharge class that transports the most of a given constituent, $Q_{1/2}$ is the discharge magnitude below which 50% of the constituent is transported over time.

Flow-frequency characterizations required for these analyses generally employ techniques that also assume stationarity in flow time series. However, it is now widely recognized that discharge magnitude/frequency behavior is also prone to non-stationarity, which can be the result of climatic cycles (Potter, 1958; Pelletier and Turcotte, 1997). On the west coast of the United States, El Niño Southern Oscillation (ENSO) cycles have been shown to cause interannual to decadal scale patterns in river discharge behavior due largely to steering of moisture convection from the tropical western Pacific. To account for the effect of climate cycles, peak annual discharge series subdivided by climatic states can be used to assess differences in peak discharge frequency between alternating climatic conditions, such as ENSO phases (Kahana et al., 2002).

The objectives of this study were to investigate the effects of antecedent hydrologic conditions and ENSO climate cycles on the estimation of suspended sediment load, Q_e, and $Q_{1/2}$ of the Salinas River in central California. Suspended load estimates from methods accounting for decadal scale suspended sediment behavior were also compared to those estimated without acknowledging temporal dependence. This work adds to a growing body of international research underscoring the importance of temporal dependence in suspended sediment behavior on multi-decadal sediment flux estimates, the diversity of mechanisms behind these dependencies, and serves as an example of small mountainous river behavior in a dry-summer subtropical climate.

2. Study site

The Salinas River drains a ~11,000 km^2 portion of the Central Coast Ranges of California from a maximum relief of ~1900 m with a mean discharge (Q_{mean}) calculated from the period of record (1930–2011) as 11.6 m^3/s. The regional climate is dry-summer subtropical, and most annual precipitation originates from winter storms, the largest of which are generally produced during strong El Niño years (Farnsworth and Milliman, 2003; Andrews et al., 2004). Three dams were emplaced on the mainstem and two major eastern tributaries previous to the initiation of suspended sediment sampling (Fig. 1). This study was based on data obtained from the two lowest USGS hydrologic gauging stations in this basin: Salinas River near Spreckels (gauge # 11152500) and Salinas River near Chualar (gauge # 11152300), hereafter referred to as S1 and S2, respectively (Fig. 1).

Three previous studies have estimated lower Salinas suspended sediment loads. Inman and Jenkins (1999) conducted a regional scale study on suspended sediment flux from central and southern California coastal rivers with a focus on episodic events and their relationship to regional climate cycles. They found that large events with recurrence intervals of 5–10 years dominated sediment transfer from the rivers in this region, including the Salinas, and that multi-decadal scale wet and dry cycles lead to concomitant increases and decreases in suspended sediment flux to the ocean, respectively. Their approach to calculating suspended sediment load utilized a rating curve constructed from data at S1 collected by the USGS from water years 1969–1979, which they applied to monthly averages of daily water discharge from 1944–1995, resulting in an estimated average annual suspended sediment load of 1.7 Mt/yr. Farnsworth and Milliman (2003) also examined the role of large discharge events in the estimation of total suspended sediment load at S1, and used the same set of S1 USGS data to compute a power law rating curve that was then applied to daily discharge data from 1930 to 2000 for an average annual suspended sediment discharge of 3.3 Mt/yr. Farnsworth and Warrick (2007) estimated lower Salinas fine sediment (clay and silt) load as part of a larger study on the flux of fine sediment to the California coast. The 1969–1979 S1 dataset was again employed, fitted in this case with a local regression (LOESS) rating technique, and then applied to the 1930–2004 discharge record for an average annual fine sediment discharge of 1.75 ± 0.9 Mt/yr.

3. Experimental overview

The experimental approach was to estimate independent loads for suspended fine- and sand-sized sediment, each through either (i) a single rating curve based on the entire temporal domain, (ii) separate rating curves for each respective period of persistent suspended sediment behavior, or (iii) a multiple linear regression rating curve incorporating indices describing antecedent hydrologic conditions previously found to influence suspended sediment behavior in the lower Salinas River (Gray et al., 2014a and b). The estimates involving antecedent hydrologic conditions were compared to decadal behavior-based estimates to further assess the role of antecedent conditions in decadal scale patterns. All estimates were then placed in the context of ENSO cycles and assessed using magnitude frequency analyses to examine the discharges responsible for moving most of the sediment through the lower Salinas.

4. Data

A brief summary of the data used for this study follows. For in depth reporting on available suspended sediment, water discharge and precipitation data see Gray et al. (2014a). The USGS collected

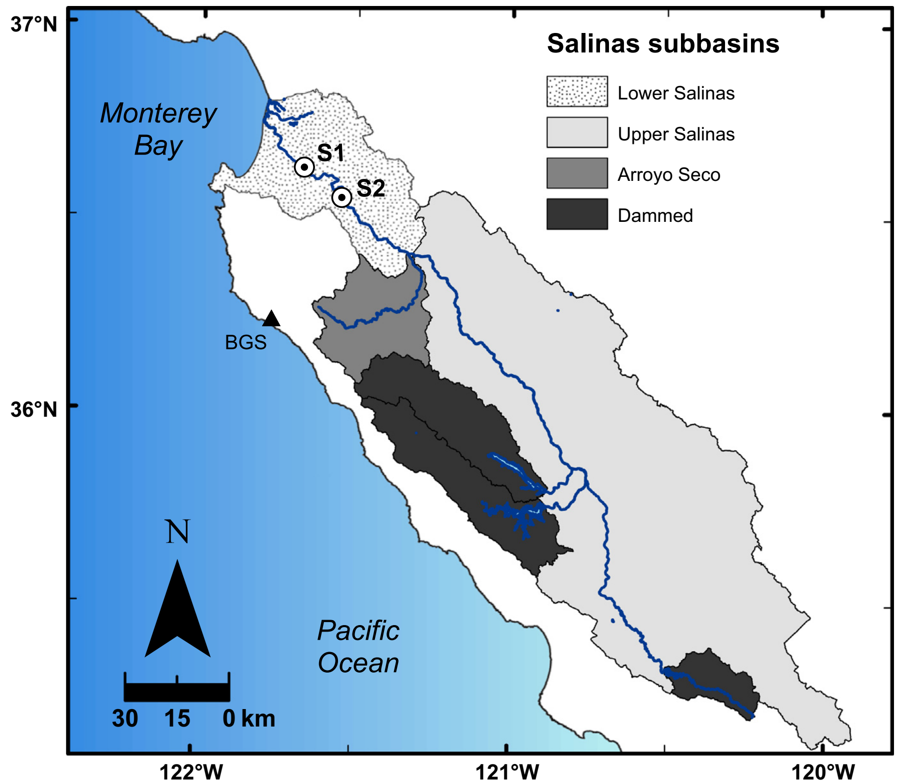

Fig. 1. The Salinas River watershed. The locations of USGS hydrologic gauging stations are marked with dotted circles and identification codes. Identification codes S1 and S2 correspond to gauge names: *Salinas R. near Spreckels* and *Salinas River near Chualar* (USGS gauge numbers 11152500, 11152300), respectively. The NOAA precipitation gauge is indicated with a black triangle and the label BGS, which stands for gauge name Big Sur State Park.

flow-integrated (depth and width integrated) suspended sediment samples from the Salinas at locations corresponding to the S1 and S2 gauges during 1967–2010, while the authors collected near-surface samples during 2008–2011 (USGS NWIS; Gray et al., 2014a). Only USGS suspended sediment data with associated instantaneous Q and particle size data was included in this study. Multiple samples collected consecutively at constant discharge were combined into single samples through simple averaging of parameters. Most USGS samples were processed for particle size distribution by sieving to establish the relative contribution of fine (Diameter (D) < 63 μm) and coarse (D > 63 μm) fractions. The concentration of fine suspended sediment (C_{SSf}) for was calculated as:

$$C_{SSf} = \frac{C_{SS} \times (\%\ \text{particles} < 63\ \mu\text{m})}{100} \quad (1)$$

where C_{SS} is total suspended sediment concentration. The concentration of sand-sized suspended sediment (C_{SSs}) was obtained by subtracting C_{SSf} from C_{SS}.

Samples were collected by the authors as per Warrick et al. (2012), with the following modifications. Samples were retrieved from the water surface at cross-channel stations of ~one-quarter, one-half, and three-quarters wetted channel width. Two 1-L samples from each cross-channel station were collected for (i) (C_{SS}) and (ii) particle size distribution analysis. The first 1-L replicate for each sample was measured and then filtered through pre-weighed, combusted, Whatman GF/A, 0.7 μm glass fiber filters. All filters were dried at 60 °C for >24 h, cooled to room temperature under vacuum in a desiccator, and then weighted to ±0.0001 g. Sample sediment mass was calculated by subtracting filter mass from total mass. The C_{SS} was calculated by dividing sample sediment mass by initial sample volume.

The second 1-L replicate was used for particle size distribution analysis. Each sample was centrifuged at 3250 g in 500-mL bottles for 10 min, and the supernatant was discarded. The remaining sediment was transferred to 150-mL beakers and treated with unheated and heated 30% H_2O_2 aliquots to remove organic materials, dispersed with sodium metaphosphate solution, and run through a Beckman-Coulter LS 230 (Beckman Coulter Inc., Fullerton, CA, USA) laser diffraction granulometer using polarization intensity differential scattering (PIDS) as per Gray et al. (2010).

Coarse suspended sediment particles were expected to be underrepresented as suspended sediment samples were collected from the surface of the river. Sediment suspension calculations by particle size based on the characteristics of the highest and lowest flows showed that fine particles should be uniformly distributed throughout the vertical profile (Rouse, 1937; Hill et al., 1988). For this reason, analysis of samples collected for this study was restricted to fine particles of D < 63 μm. Values for C_{SSf} were calculated for samples containing coarse sediments using Eq. (1).

The effects of the inclusion of two sampling sites and the selection of certain samples for particle size distribution analysis by the USGS were found to not bias the ensuing analyses. No major changes in channel morphology nor intervening tributaries are present between S1 and S2. For further details on bias analyses, see Gray et al. (2014a, Appendix A).

Sample associated discharges were instantaneous or computed from linear interpolation of associated 15-min discharge data. Daily discharge data from S1 were available for 1930–2011 and were used for suspended sediment load calculations. Historic El Niño activity was characterized in this study by (i) the Oceanic Niño Index (ONI), an aggregate measurement of sea surface temperature defects and (ii) the extended Multivariate El Niño Index (MEI.ext), which incorporates the signals of several ENSO indices (Pedatella and Forbes, 2009; Wolter and Timlin, 2011). The National Oceanographic and Atmospheric Administration's three-month running average data for ONI were used for the interval 1950–2011, and MEI.ext for 1931–1950.

5. Suspended sediment rating curve development

Available C_{SS} and associated Q data were used to model the dependence of C_{SS} on Q for the system (hereafter referred to in the form of $C_{SS} \sim Q$) after log-transformation using (i) linear, (ii) LOESS and (iii) multiple regression techniques. Linear (LR) and LOESS techniques were applied as single curves fitted to data from the entire temporal domain, and through a temporally stratified approach whereby multiple curves were fitted to discrete temporal domains of persistent suspended sediment – discharge behavior.

5.1. Linear regression and LOESS rating curves

A log-linear sediment rating curve describes the $C_{SS} \sim Q$ relationship as:

$$\log(C_{SS}) = \log(a) + b\log(Q) + \varepsilon \tag{2}$$

where a is the offset of the linear curve, b is the slope and ε is the error function. To avoid potential bias from the systematically poor fit of log-linear curves previously found for the Salinas River, LOESS rating curves for suspended fines (C_{SSf}) and sand (C_{SSs}) were also computed, using the smoothing parameter $\alpha = 0.75$, and 2nd degree polynomials (Cleveland, 1979; Cleveland and Devlin, 1988; Helsel and Hirsch, 2002; Gray et al., 2014a).

Log-linear and LOESS rating curves constructed for the lower Salinas C_{SSf} and C_{SSs} datasets over the entire temporal domain showed that linear curves fail to account for the curvature in the $C_{SS} \sim Q$ relationship at high and low Q (Table 1, Fig. 2). For this reason, LOESS curve residuals (the difference between observed and fitted values) were used to identify periods of high or low C_{SS} (see below).

5.2. Temporally zoned rating curves

Identification of persistent periods of high or low C_{SS} behavior was established in previous work (Gray et al., 2014b). Determination of which periods exhibited significantly distinct rating curves is accomplished here through ANCOVA analysis. Periods were previously identified on the basis of the local slope of sequentially summed $C_{SS} \sim Q$ residuals obtained from total temporal domain LOESS curves. Positive or negative behavior was recognized by positive or negative slopes on the sequentially summed residual curves maintained over ranges of residual values $\geqslant 3$ times the standard deviation of the residuals (Fig. 3). Zones of high C_{SSf} were identified from 1967–1979, and 1990–1993, with lower

Table 1
Suspended sediment rating curves.

Linear regression and LOESS rating curves						Shapiro–Wilk Normality Test		Log bias correction factor (BCF_l)		
Size	Time period	Model	Model equation	R^2	RMSE[a]	W	P-value[c]	Ferguson	Duan	$(F+D)/2$[e]
Fine	Total range (1967–2011)	LR	$\log C_{SS} = 1.569 + 0.713\log Q$	0.55	0.61	0.97	***	1.530	3.365	2.447[b]
		LOESS	–	–	0.59	0.96	***	1.489	3.167	2.328[b]
	1967–1979	LR	$\log C_{SS} = 1.896 + 0.634\log Q$	0.56	0.57	0.99	Normal	1.448	2.316	1.882[b]
		LOESS	–	–	0.56	0.99	Normal	1.435	1.565	1.500[b]
	1980–89, 1994–2011	LR	$\log C_{SS} = 1.326 + 0.651\log Q$	0.6	0.43	0.98	*	1.240	1.768	1.504[b]
		LOESS	–	–	0.42	0.98	*	1.226	1.346[b]	1.286
	1990–1993	LR	$\log C_{SS} = 2.233 + 0.850\log Q$	0.45	0.78	0.95	*	2.021	2.494	2.496[b]
		LOESS	–	–	0.81	0.92	Normal	2.133	2.553	2.343[b]
Sand	Total range (1967–2010)	LR	$\log C_{SS} = 0.726 + 0.920\log Q$	0.69	0.60	0.98	*	1.511[b]	4.073	2.792
		LOESS		–	0.55	0.97	**	1.411[b]	3.097	2.254
	1967–1986	LR	$\log C_{SS} = .670 + 0.947\log Q$	0.70	0.60	0.97	**	1.511[b]	4.224	2.867
		LOESS	–	–	0.52	0.97	**	1.364[b]	2.755	2.059
	1987–2010	LR	$\log C_{SS} = 0.228 + 1.125\log Q$	0.71	0.53	0.97	*	1.388[b]	2.391	1.890
		LOESS	–	–	0.48	0.99	Normal	1.305[b]	1.716	1.511

Multiple linear regression rating curves								Shapiro–Wilk normality test		Log bias correction factor (BCF_l)		
Size	Time Period	Model	Variables	Coefficients	VIF[d]	R^2	RMSE	W	P-value	Ferguson	Duan	$(F+D)/2$
Fine	Total range (1967–2011)	MLR	–	–	–	0.65	0.53[a]	0.97	***	1.384	2.782	2.083[b]
			Intercept	1.459	–		6.3E−02					
			log Q	0.677	1.42		3.7E−02					
			Q_1 *Time*	−2.12E−03	1.34		3.4E−04					
			Q_{114} *Time*	5.71E−04	1.15		6.4E−05					
			ΔQ	7.75E−04	1.09		3.3E−04					
Sand	Total range (1967–2010)	MLR	–	–	–	0.76	0.52[a]	0.96	***	1.368[b]	4.350	2.859
			Intercept	0.9819	–		0.10					
			lq	0.8255	1.31		3.9E−02					
			$\Sigma Q0.1$, *110 day*	−2.66E−03	1.42		1.0E−03					
			Q_{400} *Time*	−1.77E−04	1.54		3.9E−05					
			current Wy	1.46E−04	1.40		6.8E−05					
			previous Wy	1.54E−04	1.34		7.2E−05					

[a] Indicates root mean squared error (RMSE) values for the entire model. All RMSE values reported in log units.
[b] Indicates log bias correction factors (BCF_l) found to most closely estimate observed mean *CSS*. These values were used in subsequent Q_{SS} estimations. All BCF_l values reported in mulitplicative form.
[c] Shapiro–Wilk test result P-value ranges: normal $\geqslant 0.5$; $0.5 > * > 0.001$; $0.001 > ** > 1E{-}5$; $1E{-}5 > ***$.
[d] Variance inflation factor (VIF) values close to 1 indicate little collinearity issues between variables in multiple regressions, while VIF values near 5 or greater would indicate considerable collinearity.
[e] $(F + D)/2$ = the log bias correction factors (Ferguson + Duan)/2.

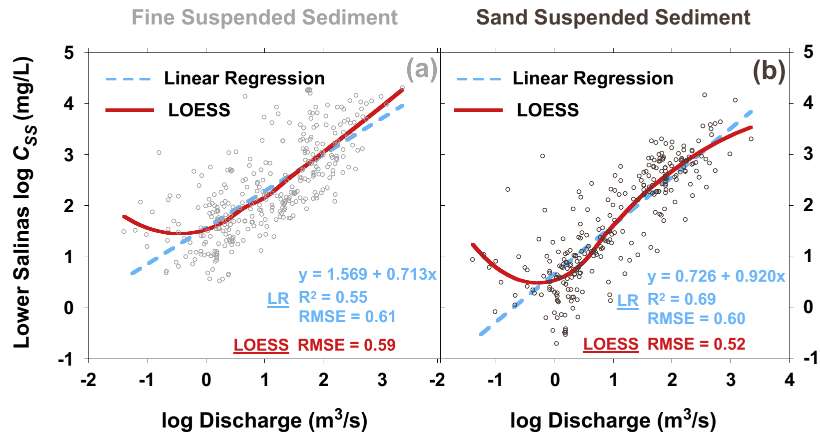

Fig. 2. Linear regression and LOESS rating curve models of C_{SS}–Q behavior in log–log space for (a) fine and (b) sand sized sediment with sample values.

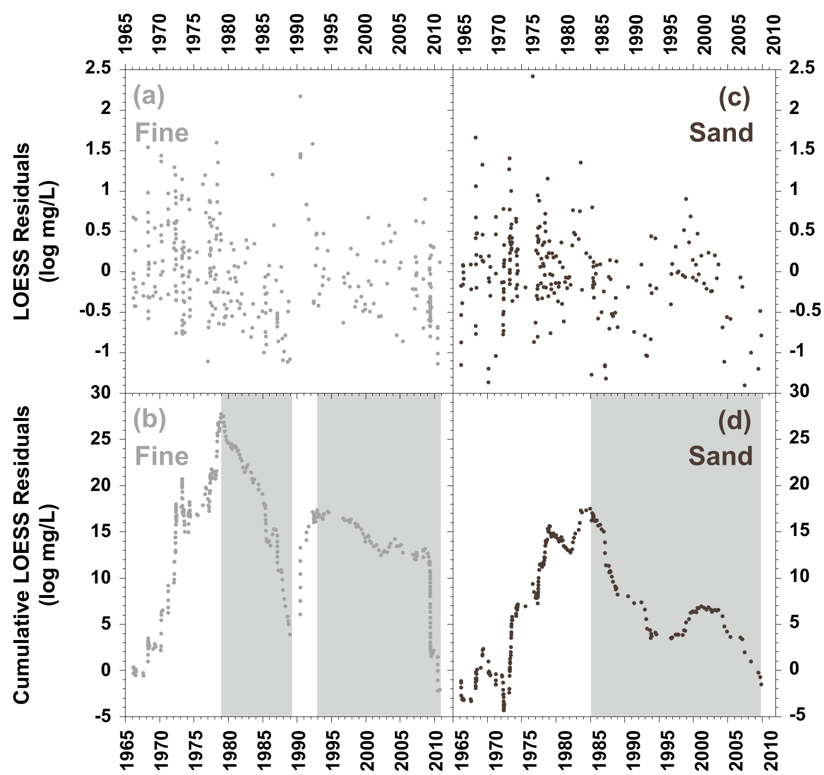

Fig. 3. Plots of (a and b) fine and (c and d) sand LOESS residuals, and LOESS residuals sequentially summed over time. Gray shading indicates zones of persistent negative residual behavior, un-shaded zones are positive.

concentrations from 1980–1989, and 1994–2011. The C_{SSs} was persistently high from 1967–1986, and low from 1987–2011.

Here positive and negative temporal zones were used to define subgroups of the C_{SSf} and C_{SSs} datasets, which were each fitted with linear regression rating curves after log transformation of C_{SSf} and Q values. An ANCOVA method was used to compare the C_{SSf} and C_{SSs} subgroups for statistically significant differences in rating curve slope and offset. For a detailed treatment of the ANCOVA approach to comparing rating curves, see Gray et al. (2014a).

All linear regression rating curves for fine sediment periods appeared to be parallel, with the exception of 1990–1993, with higher offset for positive cumulative residual zones, and lower offset for negative zones (Fig. 4a). Conversely, the two periods for sand appeared to have differing slope and offset, with the negative cumulative residual zone displaying a lower offset, but higher slope, resulting in a convergence of rating curves at the highest values of Q (Fig. 4b). ANCOVA comparisons of fine sediment rating curves at a $p < 0.05$ significance threshold showed that the two negative cumulative residual zones (1980–89, 1994–2011) were offset equivalent, as were the two positive zones (1967–79, 1990–93), with no significant difference in rating curve slopes (e.g., all fine sediment rating curves were parallel) (Table 2).

LOESS based temporally zoned rating curves generally displayed a transition from curved to log-linear relationships found for the entire temporal domain located around 1 m^3/s (0 log units) (Fig. 5). This resulted in decreased RMSE values for LOESS curves in comparison to linear regression curves, except for the 1990–1993 fine sediment period, which displayed a small increase (Table 1). Temporally zoned linear regression models generally accounted for slightly more variance in C_{SS} than found for the linear models

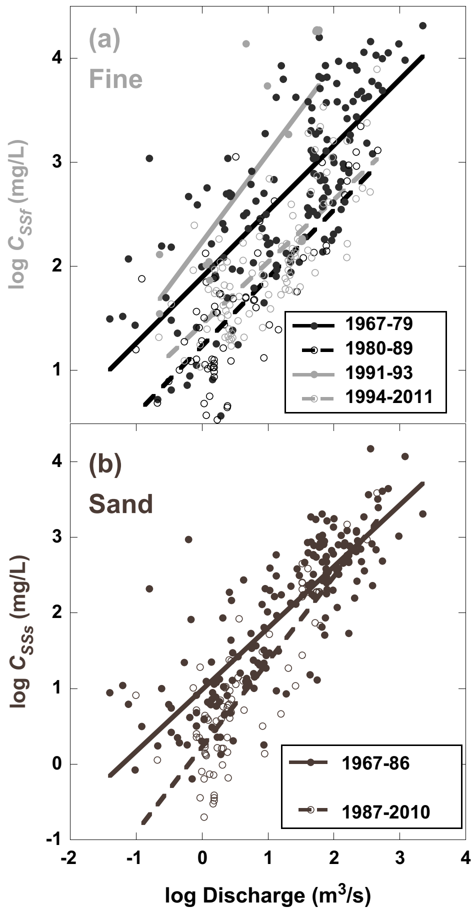

Fig. 4. Log-linear regression rating curves for (a) fine and (b) sand sized suspended sediment over temporal zones of persistent positive (solid lines) and negative (dash lines) behavior.

Table 2
Cumulative residual analysis time period rating curve ANCOVA results.

Regression pair: Sediment size	Regression pair: Time periods	Coincidence	Parallelism	Offset
Fines	1967–79 vs. 1980–89	***	P	***
Fines	1967–79 vs. 1990–93	**	P	E
Fines	1967–79 vs. 1994–2011	***	P	**
Fines	1980–89 vs. 1990–93	***	P	***
Fines	1980–89 vs. 1994–2011	C	P	E
Fines	1990–93 vs. 1994–2011	***	P	*
Sand	1967–86 vs. 1987–2010	***	***	*

C = coincident, P = parallel, and E = offset equivalent at a $P > 0.05$ threshold. Significant differences are indicated over ranges of *P*-values as:
* *P*-value < 0.001.
** *P*-value < 1E−4.
*** *P*-value < 1E−5.

based on the entire temporal domain, again with the exception of the 1990–1993 period.

5.3. Multiple regression rating curves

Stepwise multiple linear regression models were constructed with the inclusion of antecedent flow indices to account for more variation in C_{SSf} and C_{SSs} than resolved by Q alone. The authors previously examined the effects of antecedent hydrologic conditions on suspended sediment behavior in the lower Salinas River at event to interannual (Gray et al., 2014a), and decadal timescales (Gray et al., 2014b). Results of those studies showed that fine suspended sediment behavior displayed overall positive (clockwise) hysteresis at the event scale (rising vs. falling limb of the event hydrograph), with fine sediment supply suppressed by both prolonged drought periods and flushing flows of a moderate magnitude (~100–200 m^3/s). The C_{SSs} decreased with increasing elapsed time since a wide range of discharge thresholds (from 1 m^3/s to 500 m^3/s), and seasonal as well as long term (multi-annual) arid conditions also resulted in decreased C_{SSs}. Elapsed time between a given Q_j, where j indicates a given threshold discharge value from 1 to 1000 m^3/s, and the time of collection of a given suspended sediment sample is defined as Q_j *Time*. Drought is represented by $\Sigma Q_{0.1,}$ the sum of days when daily discharge $Q_d \leqslant 0.1$ m^3/s for back cast summation windows of 1–2000 days. The one-day change in Q from the day before the day of sampling was described as ΔQ_d. *Current water yield* and *previous water yield* are the annual volumetric water yields for the current water year and the previous water year respectively.

The only variables included in multiple regression calculations were those that (i) were not collinear with other variables (defined by pairwise linear correlation analysis resulting in an $R^2 < 0.8$; as per Montgomery and Peck (1992)) and (ii) resulted in statistically significant correlations with discharge-corrected C_{SS} (Chatterjee et al., 2000; Warrick and Mertes, 2009). Thus, the multiple regression rating curve for C_{SSf} employed Q_1 *Time*, Q_{114} *Time* and ΔQ_d, while that for C_{SSs} included $\Sigma Q_{0.1,\ 110\ \mathrm{days}}$, Q_{400} *Time*, *Current Water Yield* and *Previous Water Yield*. Overall R^2 values were adjusted for the increasing predictor variable pool (Chatterjee et al., 2000).

6. Suspended sediment load

6.1. Q_{SS} estimation methods

Daily suspended sediment load (Q_{SS}) was estimated for fine and sand fractions by modifying rating curve estimations of C_{SSf} and C_{SSs} to account for systematic biases and then multiplying by daily water yield values as per Warrick and Mertes (2009):

$$C_{SS} = BCF_d \cdot BCF_l \cdot C_{SS\,rating\,curve\,(Q)} \tag{3}$$

$$Q_{SS} = Q_d \cdot C_{SS} \tag{4}$$

where BCF_d corrects for bias introduced by using daily rather than instantaneous discharge and BCF_l corrects for the logarithmic transformation consequence of calculating regression parameters using geometric rather than arithmetic mean.

Estimates of $C_{SSf\ rating\ curve\ (Q)}$ and $C_{SSs\ rating\ curve\ (Q)}$ values were first obtained for all unique Q values in the S1 gauge record using linear regression, multiple linear regression and LOESS rating curves developed above. LOESS techniques alone do not allow for extrapolation beyond the domain of sampled discharge values. For LOESS rating curves supported by discharge data that fell short of the highest Q values present in the 1967–2011 S1 dataset, estimations of C_{SS} for higher Q were extrapolated by fitting a linear regression to LOESS estimations for the five highest sampled Q values. Like many coastal California rivers, low Q regime $C_{SS} \sim Q$ relationships were found to be relatively flat or convex up (e.g. Farnsworth and Warrick, 2007). Thus C_{SS} estimates for low Q were obtained by extending LOESS curves for all sample sets except fine sediment during 1991–1993 by applying a fixed mean log C_{SS} value estimated from the sampled values with Q's below the transition to positive log-linear behavior. This transition was identified by visual examination of the LOESS curve and was consistently positioned at about log $Q = 0$ (or 1 m^3/s) for all data sets. Fine sediment

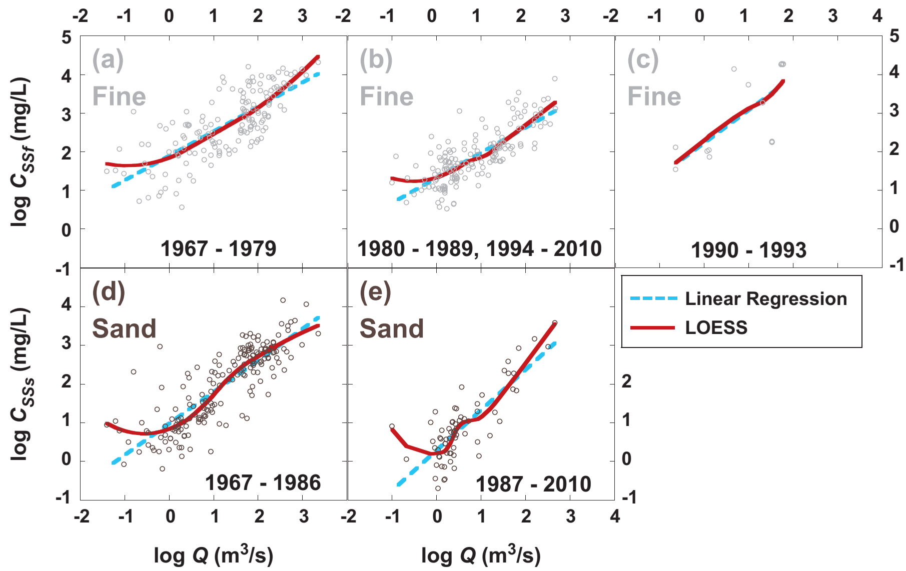

Fig. 5. Linear and LOESS rating curve models for (a–c) fine and (d and e) sand sized C_{SS}–Q behavior by temporal zones of persistent suspended sediment behavior.

samples from the 1991–1993 did not display a departure from log-linear behavior, perhaps in part due to the fact that the minimum sampled Q at 0.23 m^3/s was not as low as in all other data sets. In this case the low Q regime was estimated in the same manner explained for the high Q regime.

The parameter BCF_d was estimated to be 1.01 by comparing fine sediment loads estimated from Q_d values to fine sediment loads estimated with $Q_{15\min}$ data for water years with complete $Q_{15\min}$ time series (1992, 1994, 2001, 2003–2006, 2008, 2009) (Warrick and Mertes, 2009). BCF_l was calculated using a combination of the parametric method of Ferguson (1986), and the nonparametric 'smearing' method of Duan (1983). The Ferguson correction for log-transform bias (BCF_{lf}) is calculated as:

$$BCF_{lf} = 10^{\frac{s^2}{2}} \tag{5}$$

where s^2 is the mean squared error of the residuals. Use of BCF_{lf} is contingent upon the assumption of normality in the distribution of rating curve residuals. However, the distribution of residuals for most rating curves used in this study were found to differ significantly from normal using the Shapiro–Wilk test, where the null hypothesis is that a distribution is normal, and p-values below 0.05 were considered to indicate significant departures from normal (see Table 1) (Cohn et al., 1989; Hicks et al., 2000; Helsel and Hirsch, 2002). Thus the Duan smearing correction factor (BCF_{ld}) was also investigated, as it does not require residual distribution normality:

$$BCF_{ld} = \frac{\sum_{i=1}^{n} 10^{e_i}}{n} \tag{6}$$

where e_i is each residual value generated by subtracting the log of the observed C_{SS} values from the log of the $C_{SS\ rating\ curve\ (Q)}$ estimates and n is the number of samples (Rasmussen et al., 2009). The suitability of these factors in correcting log transformation bias was examined by computing the arithmetic mean C_{SS} for each sample set using uncorrected rating curve estimations of C_{SS}, and those corrected by either BCF_{lf}, BCF_{ld} or the arithmetic mean of the two ($BCF_{l(f+d)/2}$), and then comparing these values to the observed sample arithmetic mean C_{SS}. The BCF (or lack thereof) that resulted in a mean C_{SS} closest to the observed was chosen for inclusion in the estimation of Q_{SS}. As residuals for all rating curves were found to be homoscedastic using the nonparametric Filgner–Killeen test of homogeneity of variances, BCF_l corrections were applied uniformly to calculations across the entire discharge domain.

Sediment load uncertainty was estimated on the basis of measurement errors, rating curve uncertainty, and additional uncertainty associated with extrapolation beyond rating curve discharge domains. The original C_{SS} and Q_i measurements used to construct the rating curves have associated error, which was approximated as a total of 10% (Guy and Norman, 1970; Wass and Leeks, 1999; Yu, 2000; Farnsworth and Warrick, 2007). Rating curve uncertainty for log-linear and multiple linear regressions were calculated as per Helsel and Hirsch (2002). Error associated with LOESS rating curve uncertainty was calculated using the standard error of estimate for discreet discharge domains due to the localized regression techniques associated with this method (Farnsworth and Warrick, 2007). Error terms were propagated through each daily sediment load estimation to provide 95% confidence intervals for mean annual load estimations.

6.2. Comparison of suspended sediment load estimations

Estimated mean annual Q_{SS} ranged from 2.89 Mt/yr ± 25% (based on two LOESS rating curves: one for fines and one for sand, over the entire temporal domain) to 2.01 Mt/yr ± 106% (estimated from several temporally zoned, linear regression rating curves computed separately for fines and sands) (Table 3). Moving from entire temporal domain rating curves to temporally zoned rating curves resulted in decreased total mean annual Q_{SS} values for LOESS and linear regression methods, with reductions of 0.74 and 0.25 Mt/year, respectively. In both cases the reduction in Q_{SS} was affected by a decrease in fine sediment load (Q_{SSf}), countered to some extent by an increase in sand load (Q_{SSs}), resulting in an increase in the mean percent sand in the suspended sediment budget. Including antecedent flow indices in multiple linear regressions resulted in a 0.11 Mt/year increase to 2.37 Mt/yr ± 202% mean annual Q_{SS} relative to linear regression with Q as the lone independent variable. The increase in Q_{SS} was driven by a 0.16 Mt/year increase in sand, which was only slightly counterbalanced by a 0.05 Mt/yr decrease in fine load.

The use of LOESS as opposed to LR rating methods resulted in the decrease of model RMSE values and mean annual sediment load 95% confidence intervals (Tables 1 and 3). However, sediment load confidence intervals were much larger for time-stratified LOESS and LR estimates in comparison to non-stratified estimates (Table 3). This is despite the fact that time-stratified techniques

Table 3
Lower Salinas suspended sediment load.

Method[a]	Time period[b]	Megatons per year			95% CI[c] (%)	% Sand
		Fine QSS	Sand QSS	Total QSS		
LOESS All	1967–2011	2.42	0.47	2.89	±25	16
LOESS Tzone	1967–2011	1.39	0.74	2.13	±36	35
LR All	1967–2011	1.72	0.54	2.26	±54	24
LR Tzone	1967–2011	1.45	0.56	2.01	±106	28
MR All	1967–2011	1.67	0.70	2.37	±202	30
LOESS Tzone	1967–2011, El Niño only	2.42	1.37	3.79	±36	28
LOESS Tzone	1967–2011, La Niña & La Nada	0.20	0.12	0.33	±25	31
MR All	1967–2011, El Niño only	2.87	1.25	4.12	±167	16
MR All	1967–2011, La Niña & La Nada	0.29	0.08	0.37	±52	16
LR All	1944–1995[d]	1.40	0.44	1.83	±54	16
LR All	1930–2000[e]	1.87	0.59	2.46	±54	17

[a] LOESS is local, 2nd order polynomial regression, LR is linear regression with discharge as the single independent variable, MR is multiple linear regression multiple linear regression with hydrologic variables in addition to discharge as independent variables. 'All' indicates a single rating curve for the total temporal domain of suspended sediment samples, 'Tzone' indicates separate rating curves employed for each time period of persistent suspended sediment behavior. 'LOESS Composite' is a combination of the 'LOESS All' model applied to the 1930–1966 hydrologic record, and the 'LOESS Tzone' model applied to the 1967–2004 hydrologic record.
[b] 'El Niño only' are years determined to be in positive ENSO condition. 'La Niña & La Nada' are all other years. 1944–1995 is the time period used by Inman and Jenkins (1999) for an average annual Q_{SS} estimation, and 1930–2000 is the temporal domain utilized by Farnsworth and Milliman (2003).
[c] Confidence interval for the average annual Total Q_{SS}
[d] Temporal domain of Inman and Jenkins (1999).
[e] Temporal domain of Farnsworth and Milliman (2003).

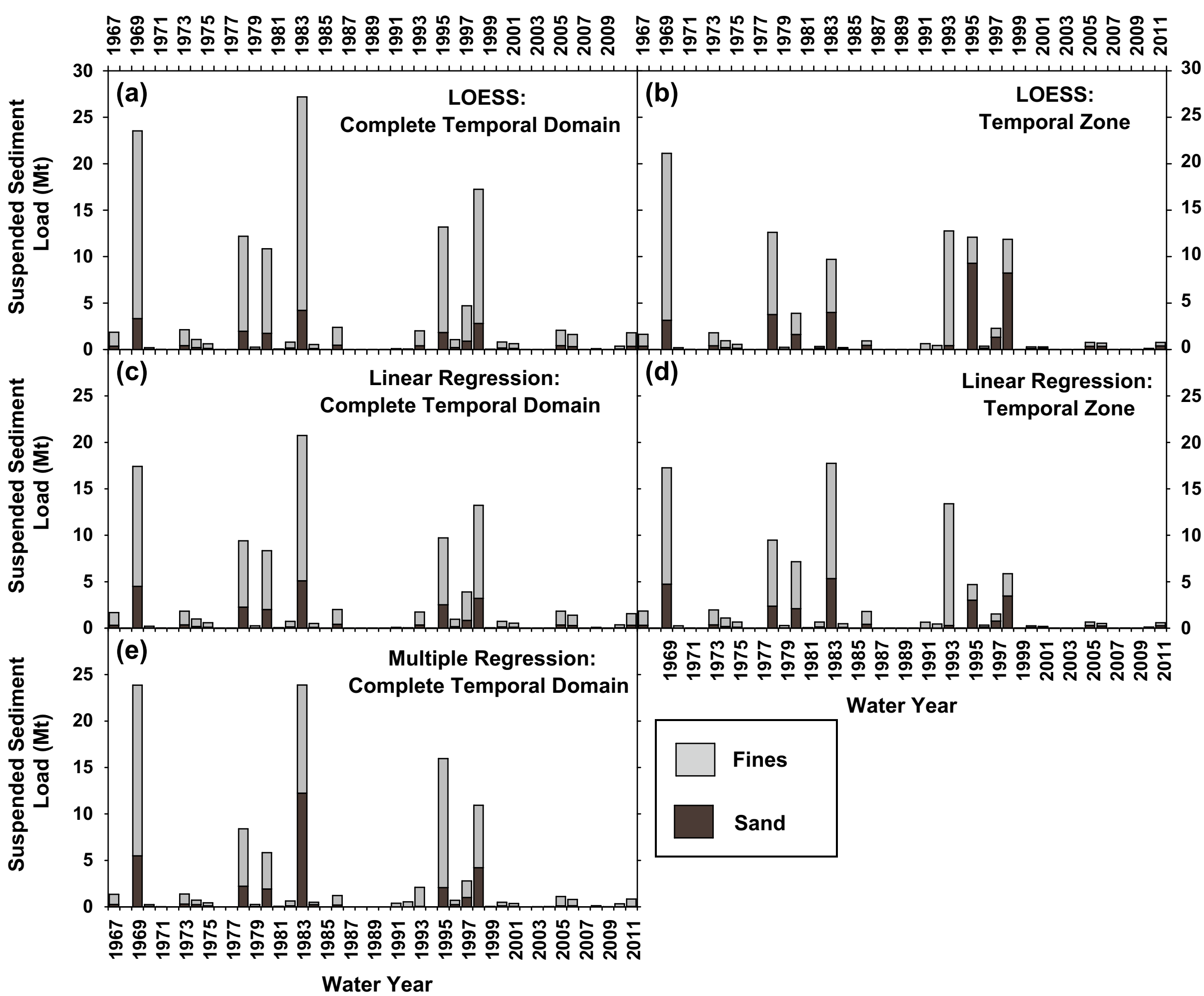

Fig. 6. Lower Salinas River annual suspended sediment discharge (Q_{SS}) by estimation method. All methods employed separate estimations for fine and sand sized sediment. (a and b) LOESS and (c and d) linear regression methods were applied as (a and c) single regression curves computed from suspended sediment data collected over the complete temporal domain of suspended sediment sampling (1967–2011), or (b and d) with different rating curves for each temporal zone of persistent residual behavior. (e) Multiple regression models were constructed using the entire temporal domain of suspended sediment data.

generally resulted in lower RMSE values, with the exception of the 1990–1993 period (Table 2). Multiple regression also resulted in much wider confidence intervals than simple linear regression, despite a similar decrease in RMSE values (Tables 1 and 3). The cause of widening confidence intervals for the time-stratified methods was due to (i) narrower observed domains for most of the time stratified rating curves exacerbating the effect of widening confidence bands toward the ends of rating curves, which was particularly impactful during periods of high discharge, and (ii) fewer observations (lower n). The cause of increased uncertainty for multiple regression estimates was due to the preponderance of wider independent variable domains than those captured by the observed cases used to construct the MR model.

Large interannual variability in both Q_{SSf} and Q_{SSs} was observed for estimates produced from all methods employed in this study, with differences between maximum and minimum annual sediment flux amounting to ~5–7 orders of magnitude (Fig. 6). This level of interannual sediment load variability is high, even for semi-arid systems, which often display a range of 1–3 orders of magnitude (e.g. Estrany et al., 2009; Warrick and Mertes, 2009; Lopez-Tarazon et al., 2012). Such a wide range of annual sediment loads is exacerbated by near zero loads during periods of multiannual droughts, which have been reported elsewhere in seasonally dry, albeit smaller Coast Ranges catchments (i.e. Tanji et al., 1980).

Linear regression and LOESS methods with total time domain rating curves produced the same rank for 33 out of 45 water years in terms of total annual Q_{SS}, including the top 18 years, whereas comparison of linear and LOESS estimates based on temporal zones resulted in only 10 years with the same rank. Moving from total temporal domain to temporally zoned rating curves using LOESS or linear regression techniques resulted in changing the rank of all but 7 or 8 water years respectively. Ranking of annual Q_{SS} magnitude was the same for simple linear and multiple linear methods in 20 out of 45 years. Despite differences in ranking, all methods of

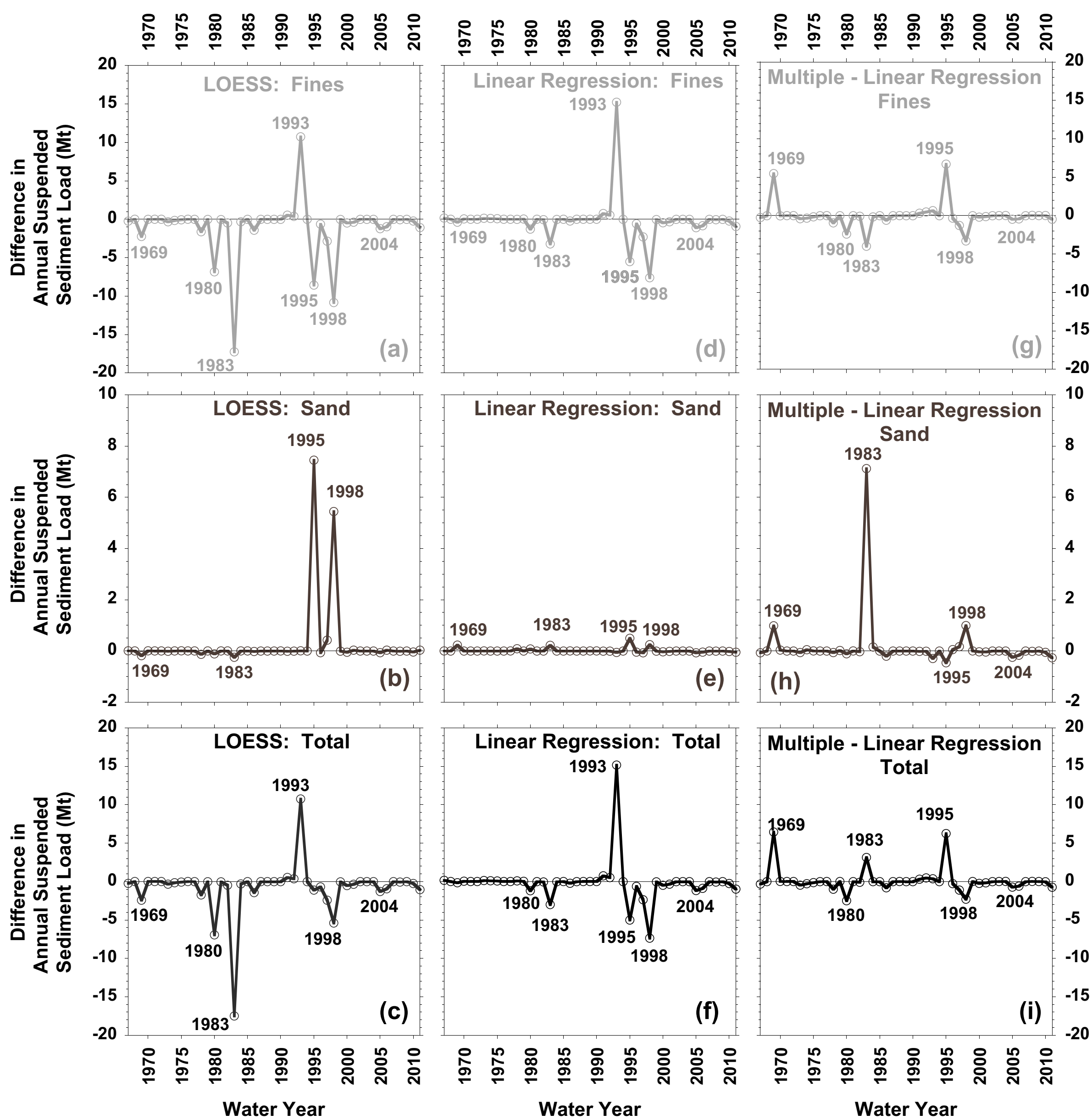

Fig. 7. Differences in annual suspended sediment discharge (Q_{SS}) estimations for fine, sand and total sediment. (a–c) LOESS temporal zone based estimations – LOESS complete temporal domain estimations. (d–f) Linear regression temporal zone based estimations – linear regression complete temporal domain estimations. (g–i) Multiple regression estimations – linear regression complete temporal domain estimations.

Q_{SS} estimation recognized water years 1969, 1978, 1980, 1983, 1995 and 1998 as among the years of highest Q_{SS}.

Some similarities were present in the differences found for Q_{SS} by water year for total temporal domain vs. temporally zoned rating curves, and total temporal domain, simple linear vs. multiple linear rating curves (Fig. 7). Patterns in total temporal domain vs. temporally zoned differences for fines and sand were similar for LOESS and linear regression techniques (Fig. 7a–f). Generally smaller magnitude differences were observed for the linear regression models (except for a large increase in fine sediment discharge in 1993), and particularly large increases in sand sized sediment were found for 1995 and 1998 LOESS temporal zone estimates (Fig. 7b). As the LOESS and linear regression sand curves for the 1987–2010 temporally zoned differed primarily over low (<1 m^3/s) and high (>100 m^3/s) discharge domains (Fig. 7e), sensitivity tests were used to remove one or the other of these differences, which showed that higher sand concentrations for the LOESS model at high Q were responsible for the resultant differences in Q_{SS} estimations (results not shown). Of the years that displayed a reduction of fine sediment discharge for linear regression temporal zone Q_{SS} estimates in comparison rating curve methods (1969, 1980, 1983, 1985, 1995–1998, 2001, 2002 2004, 2005, 2010, 2011) (Fig. 7d), all but 1969 and 1995 were also reduced by moving from simple linear regression over the total temporal domain to including antecedent flow indices for multiple regressions (Fig. 7g). Increases in fine Q_{SS} estimated for 1969 and 1995 estimated through the multiple regression approach were the two largest departures from the simple linear model, and were directly opposed to the differences obtained from time stratified simple linear regression. The multiple regression approach also resulted in small negative differences in fine sediment Q_{SS} for years 1973, 1974 and 1978, which were not observed between the single rating curve and temporally zoned models, and also produced much lower increases than found between the linear regression methods for 1992 and especially 1993. Similarities were also observed between sand linear regression (temporally zoned – single rating curve) and (multiple regression – single linear regression curve) differences (Fig. 7e and h). The years 1969, 1983 and 1998 delivered increases in sand load in both cases, while 1993, 2005, 2006 and 2011 showed decreases for both cases as well. However, the magnitude of difference was generally greater for the multiple regression – total temporal domain curve comparison, and opposite responses were observed for the years 1978, 1980, and 1995, when temporally zoned difference was positive and multiple regression difference was negative, and 1984, 1996, 1997, when multiple regression difference was positive and temporally zoned difference was negative or null.

Thus, the inclusion of antecedent flow indices in the estimation of Q_{SS} had an effect similar to that of subdividing the total temporal domain linear regression curves into roughly decadal scale zones of behavior for the later part of the record (1996–2011) (Fig. 7f and i), but did not capture the largest differences obtained through temporal zonation in the earlier part of the record, namely for years 1969, 1983, 1993, and 1995, due to large difference between multiple regression and temporally zoned linear regression in fine (1969, 1993, 1995) (Fig. 7d and g) and sand (1983, 1995) (Fig. 7e and h) estimations for those years.

6.3. Differences in Q_{SS} estimation for critical years

Four years were identified as most critical to the differences between sediment flux estimates (1969, 1983, 1993, and 1995). Further work was undertaken to evaluate the sensitivity of different estimations of Q_{SS} to different rating methods and to establish which method is in better agreement with observations.

Cumulative Q_{SS} plots were used to identify the discharge domains over which estimates from different rating methods converged or diverged (Fig. 8). Larger magnitude fine Q_{SS} values estimated from multiple regression for 1969 and 1995 were primarily the result of discharges ⩾1000 m^3/s (Fig. 8a and c). Multiple regression estimates of Q_{SSf} were lower than linear regression estimates for discharges <1000 m^3/s during 1969 and 1995, with the exception of total temporal domain linear regression estimates in 1995. In contrast, temporally zoned linear regression resulted in much higher Q_{SSf} for most of 1993, while multiple

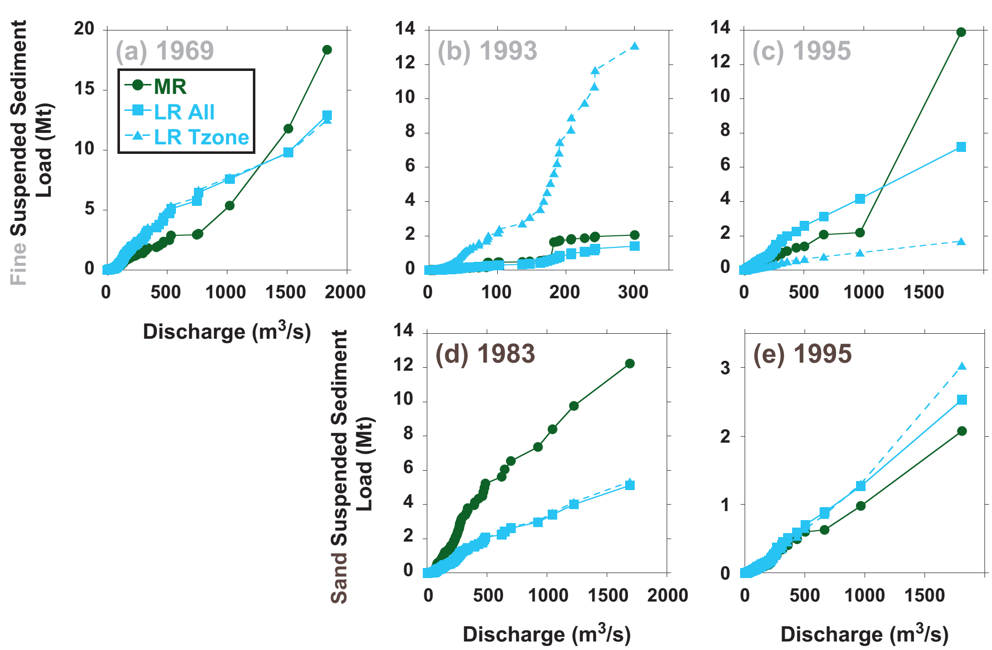

Fig. 8. Cumulative suspended sediment discharge estimates by daily water discharge magnitude for water years 1969, 1983, 1993 and 1995. Fine suspended sediment is featured in (a–c); sand sized suspended sediment in (d and e). "MR" stands for multiple linear regression including water discharge and hydrologic variables. "LR" stands for linear regressions with water discharge as the independent variable. "All" indicates a single rating curve used for the total temporal domain of sampling (1967–2011), while "Tzone" indicates separate rating curves for temporal zones of persistent suspended sediment behavioral characteristics.

regression only diverged from the total temporal domain linear estimates due to a few discharge days between ~80 and 175 m^3/s (Fig. 8b). Multiple regression Q_{SSs} estimates in 1983 were consistently higher, while simple linear methods were almost indistinguishable (Fig. 8d). All methods produced similar Q_{SSs} for 1995 up to the three days with $Q > 500$ m^3/s, after which time-stratified linear regression estimates were the highest (Fig. 8e).

Comparisons of observed C_{SS} to estimates based on multiple regression and simple linear regression were used to examine the relative efficacy of these methods (Fig. 9). For 1969, 1983 and 1995 (Fig. 9a, c–e) multiple regression values were plotted for all days between the day before and the day after the first and last sample collection dates, respectively. The plot for the 1991–1993 water years included multiple regression C_{SS} estimations for all days with non-zero Q (Fig. 9b). For water year 1969, all methods of estimating C_{SSf} plotted lower than observed values for low Q (0.16–0.24 m^3/s) and were in close agreement with observed values for ~$60 < Q < 470$ m^3/s (Fig. 9a). While both linear regression methods plotted close to observed for high Q estimates (>1000 m^3/s), multiple regression estimates were well above observed values.

It should be noted that the highest observed C_{SSf} value on record of 20,566 mg/L was collected on 2/26/1969, and thus the three high Q multiple regression estimates of C_{SSf} at 26,350–48,647 mg/L are higher than any found in 45 years of sampling. High C_{SSf} estimations for these three days were driven by high values of the antecedent flow index ΔQ (Table 4).

A more complex pattern of C_{SSf} behavior and estimations emerges for water years 1991–1993 (Fig. 9b). Observed values from water years 1991–1992 plot along a generally linear corridor described by multiple regression estimates for these two years and

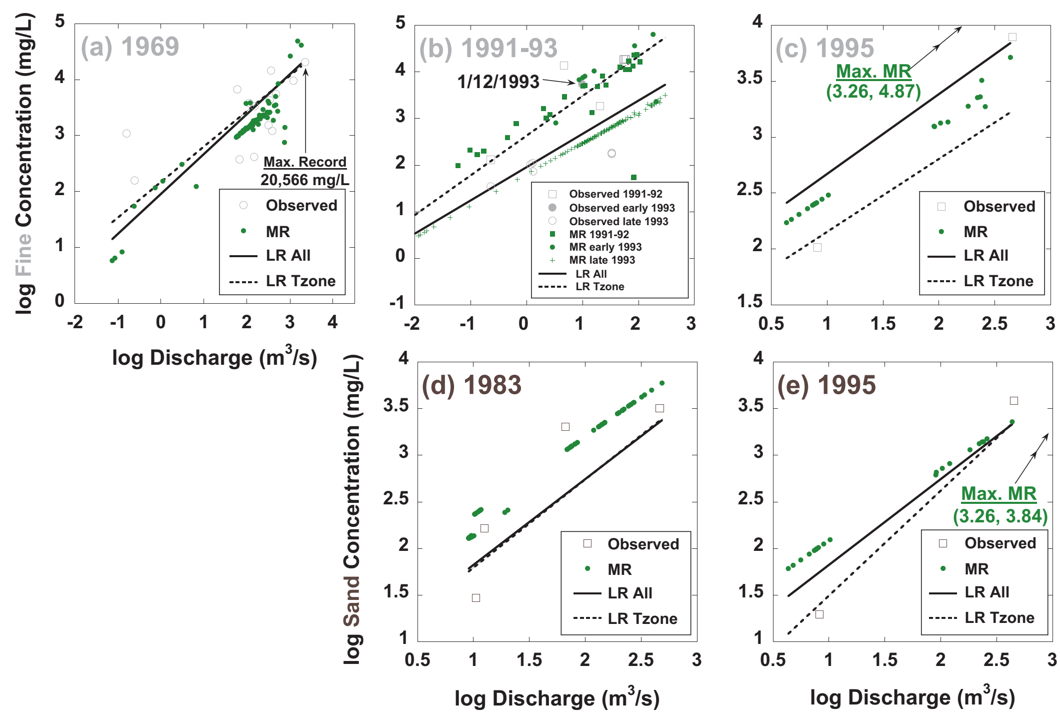

Fig. 9. Comparisons of observed and estimated suspended sediment concentrations for water years 1969, 1983, 1991–93 and 1995. Observed values are subdivided in the 1991–93 plot (b) into water years 1991–92, early 1993 (1/9–15/1993), and late 1993 (after 1/15/1993). Estimation methods plotted are multiple regression (MR), and linear regression (LR) utilizing total temporal domain rating curves (All) and temporal zone rating curves (Tzone), all of which have been corrected for log and daily discharge bias (see Section 6.1). Multiple regression estimates are shown as points values for daily discharge values corresponding to the days within the temporal domain defined by the first and last days when samples were collected in a given water year, plus one day on either end for the 1969, 1983 and 1995 water year plots (a, c–e), and all non-zero discharge days for 1991–93 (b). Linear regressions values are shown as their corresponding regression curves. "Max. MR" in (c and e) indicates the maximum daily C_{SS} estimate produced from multiple regression with corresponding (C_{SS}, water discharge) values in log units, which and double arrows indicating that they would plot outside of frame in both cases.

Table 4
Average proportional contribution of hydrologic variables[a] to multiple regression C_{SS} estimates.

Water years	Time period	Q (m^3/s)	Fine (Mt)			Sand (Mt)			
			Q_1 *Time*	Q_{114} *Time*	ΔQ	*Sum Q0.1, 110 day*	Q_{400} *Time*	*Wy Current*	*Wy Previous*
1967–1979	10/1/1966–9/30/1979	0–1834	−0.15	0.21	0.00	–	–	–	–
1980–1989	10/1/1979–9/30/1989	0–1693	−0.31	0.28	0.00	–	–	–	–
1994–2011	10/1/1993–9/30/2011	0–1812	−0.05	0.11	0.00	–	–	–	–
1969	1/27/1969, 2/26–27/1969	1022–1834	0.00	0.00	0.15	–	–	–	–
1983	Sample dates + 10 day buffers	9–487	0.00	0.02	0.00	−0.01	−0.02	0.14	0.02
1991–92, 1993 (early)	10/1/1991–1/15/1993	0–107	−0.07	0.34	0.00	–	–	–	–
1993 (late)	1/15/1993–9/30/1993	0–300	0.00	0.01	0.00	–	–	–	–
1995	3/20–28/1995	90–436	0.00	0.00	0.00	−0.03	0.00	0.05	0.00
1995	5/11–15/1995	5–9	0.00	0.01	0.00	0.00	0.00	0.08	0.00

[a] The following hydrologic variables were included: Q_1 *Time*, Q_{114} *Time* and Q_{400} *Time*, are the elapsed times since the last daily discharge ⩾1, 114 or 400 m^3/s, respectively. ΔQ is change in daily discharge. $\Sigma Q0.1$, 110 *day* is the number of days with daily discharge values ⩽0.1 m^3/s. *Wy Current* is the water yield of the water year of sample collection. *Wy Previous* is the water year before the year of sample collection.

the temporal zone linear regression line. The first observed value for the 1993 water year (collected on 1/12/1993) also fell within this zone, while observed values collected later in the year (between 3/9–9/8/1993) plotted with or below the total temporal domain linear regression curve. Multiple regression estimations of C_{SSf} were found to be highly contingent on the Q_{114} *Time* antecedent flow index, which increased steadily over this period until a discharge >114 m^3/s was reached on 1/15/1993 (Table 4). Thus, multiple regression estimates for "early" 1993 plot with the observations and temporal zone estimates for 1991–1992, while the "late" 1993 multiple regression estimates plotted with the total temporal domain linear regression and the "late" 1993 observed C_{SSf} values. Therefore the multiple regression approach seems to capture the general pattern of both inter- and intra-annual suspended sediment dynamics in this case, whereas the temporal zonation approach missed the transition to lower C_{SSf} behavior, resulting in a much higher estimation of Q_{SS} (see Fig. 8b).

Only two samples were collected in 1995 at low (8.2 m^3/s) and moderately high (453 m^3/s) discharge, which limited the comparisons between estimated and sampled C_{SS} values. both fine (Fig. 9c) and sand (Fig. 9e) multiple regression estimates followed a similar linear pattern, plotting above the low discharge observation and below the high discharge observation. The multiple regression estimations for fine sediment plotted between the linear methods, whereas multiple regression estimates of sand were greater than both linear regression methods. The maximum daily discharge in 1995 resulted in a multiple regression estimate of 11.72 Mt of fine sediment flux in a single day (Fig. 8c). In contrast, steep linear regression sand rating curves both led to higher annual Q_{SS} estimates due to higher sediment loads than found with multiple regression (Figs. 8e and 9e).

Consistently high multiple regression estimates of C_{SSs} across the discharge domain in 1983 resulted in high Q_{SSs} estimates. (Figs. 8d, and 9d). Multiple regression estimates of C_{SSs} also more closely fit the small set of observed values than the estimations from linear regressions. Sand Q_{SS} estimates were increased in 1983 multiple regression estimates due to the high current water yield value, and low values for the (Sum $Q_{0.1}$, 110 day) and Q_{400} Time indices (Table 4).

7. Magnitude and frequency analysis of Q and Q_{SS}

7.1. Methods of magnitude and frequency analysis

Determination of effective discharge ($Q(e)$) requires the computation of the transport efficacy ($e(Q)$) of the range of discharges experienced:

$$e(Q) = Q_{SS}(Q) \cdot f_{(Q)}(Q) \tag{7}$$

where $Q_{SS}(Q)$ is the constituent discharge (in this case suspended sediment) as a function of discharge, and $f_{(Q)}(Q)$ is a representation of the probability density function (*pdf*) of discharge (Wolman and Miller, 1960; Wolman and Shick, 1967; Klonsky and Vogel, 2011). Effective discharge is the value of discharge that results in the maximum value of $e(Q)$ for a given transport constituent. Assignment of $Q(e)$ is highly dependent on the method employed for estimating the *pdf*, and recent studies have shown that switching from (i) arbitrary binning (histogram) and generalized, parametric frequency function methods to (ii) nonparametric kernel density estimations with optimized spacing yields more stable approximations of $Q(e)$ (Klonsky and Vogel, 2011). This study employed the R package 'KernSmooth' with a Gaussian kernel and the sample variance based 'oversmoothed bandwidth selector' as per Wand and Jones (1995, p. 61) to generated the kernel density estimation for the daily discharge record at S1 from 1930 to 2011 (Wand, 2012; R Development Core Team, 2013). Discharge-based estimates of fine, sand and total suspended sediment load were computed by discharge bin using each of the rating curve techniques detailed above. Effective discharge was then estimated for the aforementioned suspended sediment fractions as well as water discharge from the basin.

Half load discharge ($Q_{1/2}$) was calculated for fine, sand and total suspended sediment as well as Q by summing Q_{SS} and water yields for all unique daily discharges from 1930 to 2011 at S1, and then creating a running sum of the proportional contributions of these discharge values to the total loads of each suspended sediment constituent and water yield over the period of record. Both $Q(e)$ and $Q_{1/2}$ for suspended sediment loads and Q were compared to Q_{mean}.

7.2. Magnitude/frequency results

Transport efficacy of suspended sediment was generally characterized as highly multimodal, with many peak $e(Q)$ values of similar magnitude, producing a wide range of effective discharge estimations (Table 5, Figs. 10–12). Water yield $e(Q)$, on the other hand, was strongly unimodal with a $Q(e)$ of 9.9 m^3/s, or $\sim 0.85 \times Q_{mean}$ (Fig. 10j). As $e(Q)$ is the product of frequency and Q_{SS} for a given Q, and discharge frequency in this study is expressed as a fixed set of kernel density estimations, the differences in $e(Q)$ and resultant $Q(e)$ values are the result of differences in the formulation of Q_{SS} estimations. Fine suspended sediment effective discharge ($Q(e)_f$) ranged from 14.8 to 1979 m^3/s, with most methods producing values of either 14.8 or 460–465 m^3/s (Figs. 10a–c and 11). Sand

Table 5
Effective and half-load discharge.

Method[a]	$Q(e)$: Effective discharge[b] (m^3/s)				$Q_{1/2}$: Half load discharge[c] (m^3/s)			
	Fine[d] Q_{SS}	Sand[e] Q_{SS}	Total Q_{SS}	Water	Fine Q_{SS}	Sand Q_{SS}	Total Q_{SS}	Water
LOESS All	465	124	465	–	528	423	512	–
LOESS Tzone	1979, 460, 465	124, 1979	–	–	451	699	498	–
LR All	14.8	465	14.8	–	459	558	464	–
LR Tzone	14.8, 14.8, 465	465, 1979	–	–	298	657	385	–
MR All	1811	252	1811	–	919	617	814	–
Water yield	–	–	–	9.9	–	–	–	134

[a] All methods except 'Water yield' employed log transformed suspended sediment concentration and water discharge data. LOESS stand for low order polynomial local regression, LR = linear regression, MR = Mulitple Regression. Water yield calculations were based on daily average discharge data. 'All' indicates use of single rating curves for data over the complete temporal domain of suspended sediment data collection, 'Tzone' indicates separate rating curves applied to temporal zones, or time periods, of persistent LOESS rating curve residual behavior.
[b] Effective discharge is the water discharge magnitude responsible for the greatest flux of a given constituent over time.
[c] Half load discharge is the magnitude of water discharge where the cumulative flux of a given constituent has reached half of the total flux over the period of record.
[d] LOESS and LR Tzone $Q(e)$ estimations for fine sediment are listed in order for the following time periods: (1967–79);(1980–89, 1994–2011); (1990–93).
[e] LOESS and LR Tzone $Q(e)$ estimations for sand are listed in order for the following time periods: (1967–1986); (1987–2011).

suspended sediment effective discharge ($Q(e)_s$) was generally higher, falling between 124 and 1979 m^3/s, with multiple methods producing estimates of 124, 465 and 1979 m^3/s (Figs. 10d, e and 12). As fine sediment represents the majority of suspended sediment flux, total suspended sediment $Q(e)$ estimates were dominated by fine $e(Q)$ values, which resulted in total sediment $Q(e)$ estimates that agreed with $Q(e)_f$ for each method (Fig. 10g–i).

Cumulative discharge patterns also exhibited a wide range of behavior depending on particle size range (total, fine or sand fraction of suspended sediment) and method of Q_{SS} estimation, which resulted in a wide range of $Q_{1/2}$ estimations (Fig. 13, Table 5). However, most cumulative discharge curves displayed steeper sections from ~1 to 500 m^3/s, followed by a lower angle curve from ~500 to a high discharge value varying from ~1700 to 1800 m^3/s, after which a second steep jump the cumulative discharge curve occurred. This pattern of paired 'low' range (~1–500 m^3/s) and high range (>1700 m^3/s) rapid flux accumulation is driven by the high frequency of discharge over the low discharge

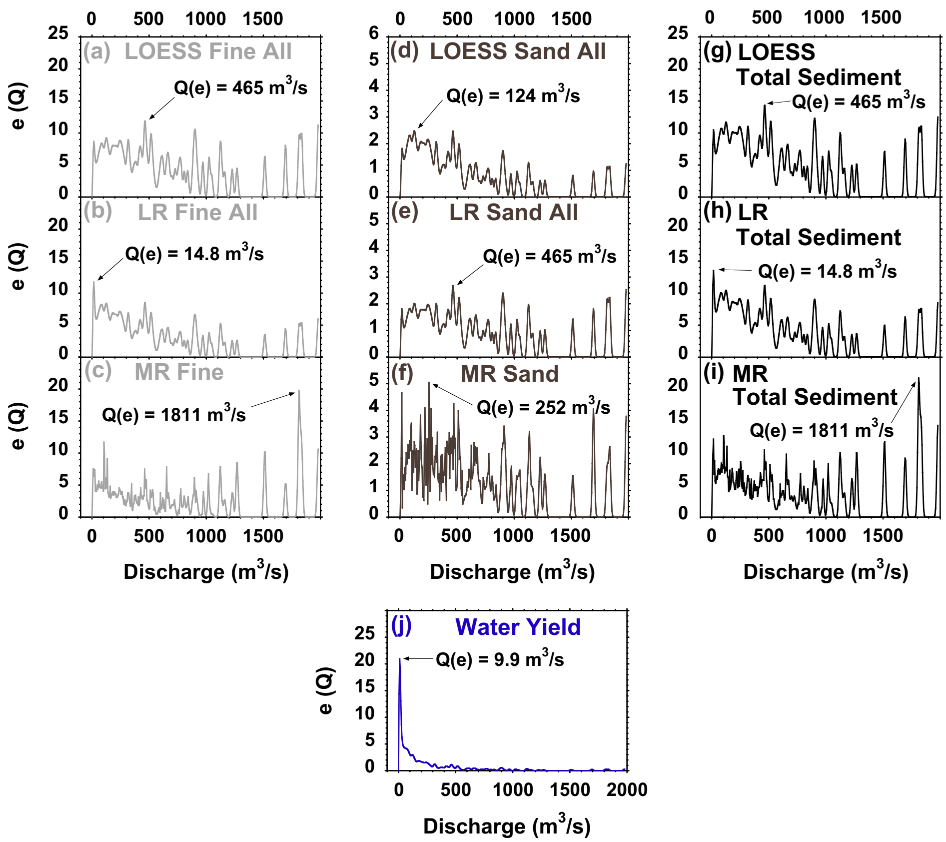

Fig. 10. Plots of discharge efficacy ($e(Q)$) for (a–c) fines, (d–f) sand, (g–i) "total sediment" (fines + sand), and (j) water yield. Effective discharge ($Q(e)$) is identified for each case. All methods for sediment flux estimation employed the complete temporal domain of suspended sediment data, as indicated by for the LOESS and LR (linear regression) plots. "MR" indicates estimation with multiple regression rating curves employing variables representing antecedent hydrologic conditions. Water yield was computed from daily discharge values.

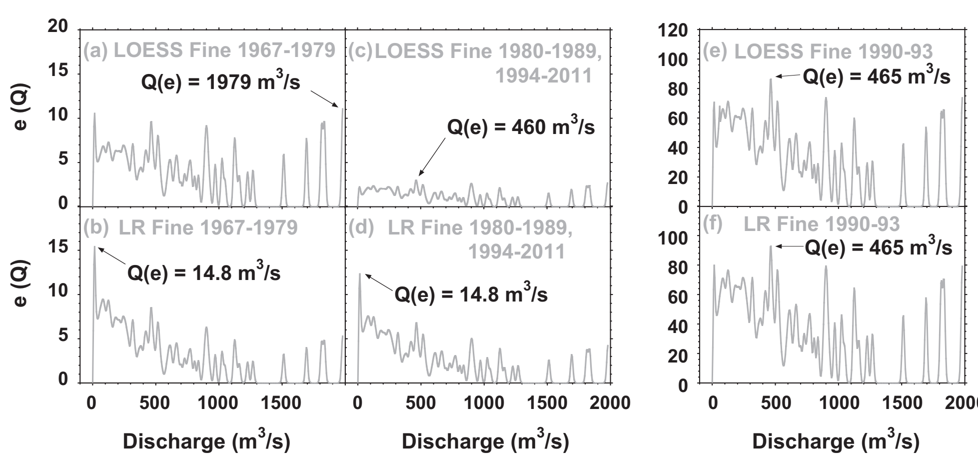

Fig. 11. Plots of fine suspended sediment discharge efficacy ($e(Q)$) for (a, c, e) LOESS and (b, d, f) linear regression estimation methods by temporal zone. Effective discharge ($Q(e)$) identified for each case.

domain, and the massive rate of sediment flux at the much less frequent, higher discharge domain. Resulting $Q_{1/2}$ for fines, sand, and total suspended sediment were between 298–919 m^3/s, 423–699 m^3/s, and 385–814 m^3/s, respectively, with variation on the basis of Q_{SS} estimation method (Table 5, Fig. 13b, d, f). The $Q_{1/2}$ for water yield (134 m^3/s) was lower than that of any suspended sediment constituent.

8. ENSO controls on flood frequency and sediment discharge

8.1. ENSO stratified flood frequency analysis

To examine flood frequency for given discharge magnitudes and climatic states, the lower Salinas (S1) peak annual water discharge record in its entirety, as well as the El Niño and La Niña data subsets were subjected to a Log Pearson III type flood frequency analysis using HEC-SSP 2.0 software with standard settings as per Bulletin 17B of the Interagency Advisory Committee on Water Data (IACWD, 1982; USACE, 2010). Peak annual discharge records for S1 were subdivided on the basis of ENSO activity into years that contained an El Niño, La Niña or neutral (La Nada) signal (Fig. 14). The presence of dominant El Niño or La Niña like conditions was defined as (MEI.ext, ONI) >0.5 or <−0.5 respectively during the general precipitation phase of the Salinas water year (October–April), and La Nada for the remaining years that did not satisfy these conditions. Years classified on this basis as ‘El Niño’ or ‘non-El Niño’ (La Niña and La Nada) were then examined in terms of annual Q_{SS}.

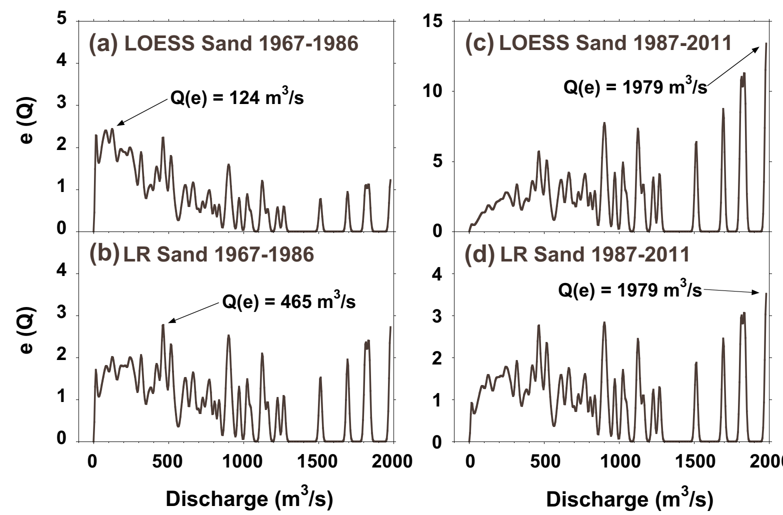

Fig. 12. Plots of sand sized suspended sediment discharge efficacy ($e(Q)$) for (a and c) LOESS and (b and d) linear regression estimation methods by temporal zone, for discharge classes generated from kernel density estimations, with effective discharge ($Q(e)$) identified for each case.

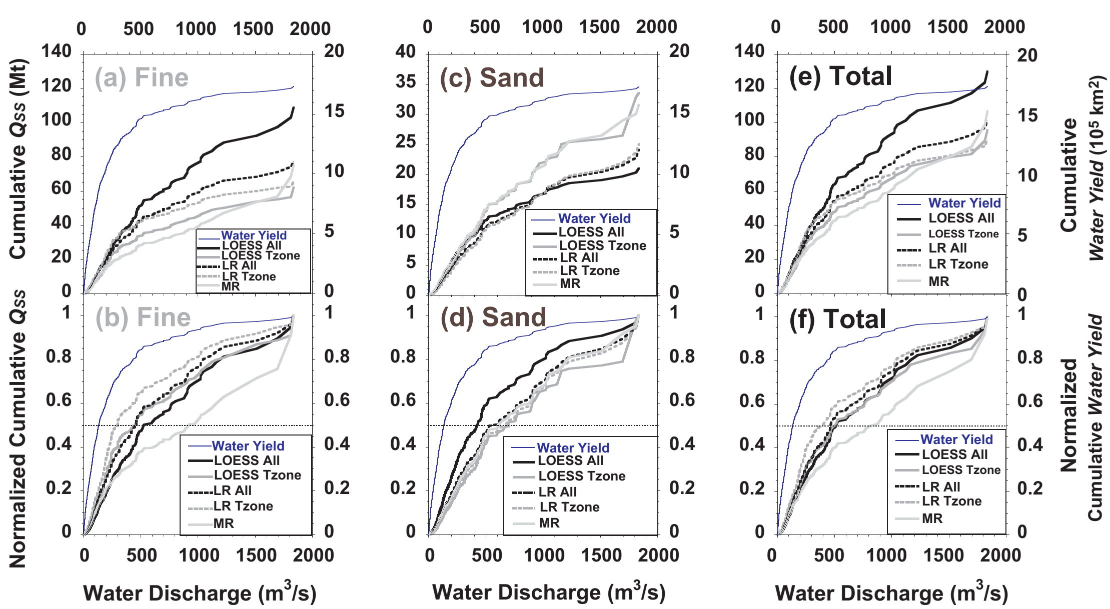

Fig. 13. Cumulative discharge curves for the lower Salinas River representing (a and b) fine, (c and d) sand, and (e and f) total suspended sediment discharge estimates for the period of (1967–2011) plotted by method and sequentially summed by increasing water discharge. Water yield over the same period summed by water discharge magnitude are included in each plot for reference. Plots (b, d, and f) show values normalized by corresponding cumulative suspended sediment discharge.

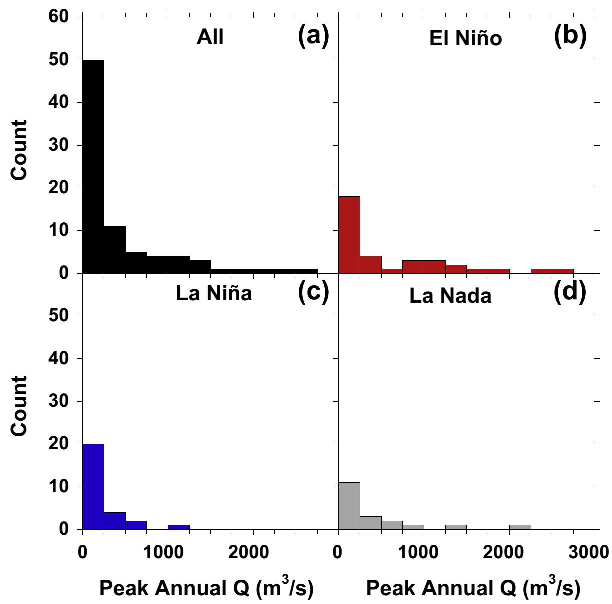

Fig. 14. Histograms of peak annual flow values at S1 for (a) the total record, (b) El Niño, (c) La Niña, and (d) La Nada years.

8.2. The role of ENSO in Q_{SS}

Flood frequency analysis stratified by ENSO phases yielded almost identical curves in the 50–95% exceedance range (corresponding to an annual peak flow of ~1–200 m^3/s) (Fig. 15). However, flood frequencies diverged for the rarest peak magnitudes, with 100-year floods estimated at ~6000 m^3/s for El Niño years as compared to only ~2000 m^3/s for La Niña years. As inter-decadal scale sediment flux in the Salinas River is largely driven by these rare, high discharge events, the ENSO phase effects on flood frequency were also found to have a large effect on average annual Q_{SS} (Table 3). Average sediment flux estimates were ~10 times larger for the collection of El Niño years (3.79, 4.12 Mt/year) vs. non-El Niño years (0.33, 0.37 Mt/year) based on time-stratified LOESS curves and multiple regression, respectively (Table 3).

9. Discussion

9.1. Suspended sediment load estimation

The case of the Salinas River provides a clear example of the effects of temporal dependence in the C_{SS}–Q relationship on suspended sediment discharge estimation. Use of the entire 45 year suspended sediment record with single rating curve models resulted in consistently higher estimates of mean annual Q_{SS} for LR and LOESS estimates in contrast to the use of separate rating curves for each period of persistent positive or negative residual behavior.

Because even small to moderate sized river systems such as the Salinas may express decadal scale persistence in flow and suspended sediment behavior (Pelletier and Turcotte, 1997; Inman and Jenkins, 1999; Horowitz, 2003; Gray et al., 2014b), a sampling interval of a single decade can lead to under or over estimation of multi-decadal sediment flux averages if samples are collected from one period of persistent behavior. Comparison between the results of this and previous studies illustrates the effects of persistent periods of suspend sediment behavior on sediment load estimates in relation to the rating curve base period of observed data. All methods of mean annual Q_{SS} estimation in this study fall between the low estimate of Inman and Jenkins (1999) and high estimate of Farnsworth and Milliman (2003), both of which were based on log-linear regressions of USGS suspended sediment samples at S1 from the 1970s. A more specifically comparable application of the log-linear regression developed in this study based on the 1967–2011 record of C_{SS} to the periods of discharge record utilized by Inman and Jenkins (1999) and Farnsworth and Milliman (2003) resulted in average annual Q_{SS} that was 8% greater and 25% less than the two previous studies respectively (see Table 3). Both of these previous studies utilized rating curves based on data from the 1970s, a decade of persistently high suspended sediment concentration, which served to increase their estimates of sediment load. However, Inman and Jenkins (1999) used monthly average discharge values, which contributed to their low estimate of 1.7 Mt/yr, as monthly averaging of discharge values decreases estimates due to the generally log-linear $C_{SS} \sim Q$ relation. Additionally, Inman and Jenkins (1999) did not include a bias correction factor for logarithmic transformation in their methods, which further

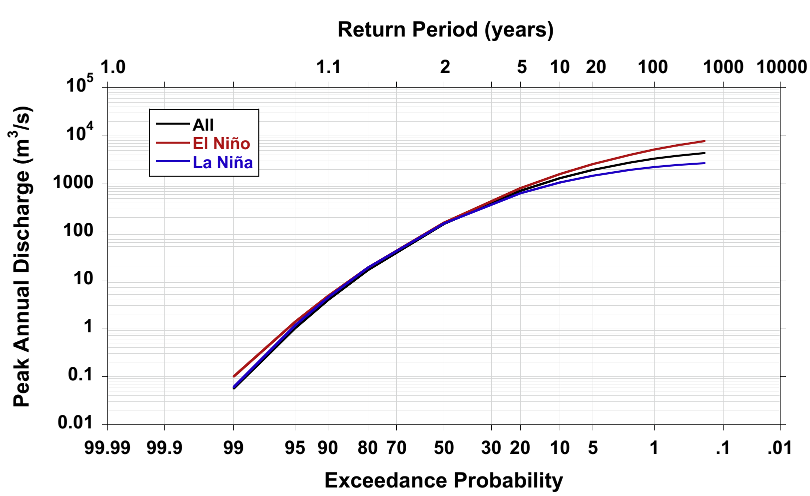

Fig. 15. Flood frequency analysis results for the lower Salinas at gauge S1 using Bulletin 17B calculations applied to peak instantaneous discharge values for the hydrologic record 1930–2011. "All" indicates the probability curve calculated from the entire data set. "El Niño" and "La Niña" indicate curves based on sub-sets of peak discharge defined by water years dominated by either El Niño or La Niña like conditions.

lowered their estimates. Similar to the study presented here, Farnsworth and Milliman (2003) used daily Q in their computations, and likely a Ferguson-based correction factor for log bias. Therefore their average Q_{SS} result of 3.3 Mt/year (1930–2000) estimated from a 1969–1979 base period, in contrast to an LR estimate of 2.46 Mt/year (1930–2000) using the 1967–2011 base period, serves as a further example of limited base period resulting in increased estimated Q_{SS}. The high Farnsworth and Milliman (2003) estimate is primarily the result of assuming stationarity suspended sediment behavior at the inter-decadal scale.

In agreement with studies of other west coast river in the United States, this study found that the $C_{SS} \sim Q$ relation is described better by a log LOESS curve than a log-linear curve (Williams, 1989; Farnsworth and Warrick, 2007; Warrick et al., 2013). Transitioning to a LOESS curve led to increases in average Q_{SS} estimates due to higher fine C_{SS} values over the low (<1 m^3/s) and high (>100 m^3/s) discharge domains relative to linear regression predictions. Including antecedent flow indices into multiple regression also increased the overall estimation of Q_{SS}. There was evidence of better fit from the multiple regression method for some years when LOESS temporal zone curves were lower than observed values (e.g., 1991–1993) including years critical to overall sediment flux, such as 1983. However, there were also indications that multiple regression estimates were over predicting C_{SS}, particularly in 1969.

Transitioning from LR to LOESS methods led to a decrease in rating curve RMSE values and smaller mean annual Q_{SS} 95% confidence intervals. However, accounting for non-stationary C_{SS}–Q relationships through temporally stratified rating curves increased the confidence interval size for both LR and LOESS models, as did the inclusion of additional hydrologic indices into the linear model. These approaches were based on statistically significant changes in C_{SS}–Q relationships in terms of both time and hydrologic forcings, and are useful for indicating that persistent behavior and antecedent conditions can play a role in determining sediment load. For example, the efficacy of the multiple regression model in capturing the transition of C_{SS} response at the end of the drought in the early 1990s shows that such techniques have promise beyond that of single base period and time-stratified models. Some similarities in the Q_{SS} estimations of time-stratified and multiple regression models also provided further support for previous findings that decadal scale persistence in C_{SS}–Q behavior in the Salinas River was largely controlled by patterns in antecedent basin conditions (Gray et al., 2014b). Furthermore, the fact that the system displays persistent behavior violates a major assumption underlying the use of individual, single base period rating curves, and calls into question the tighter confidence intervals evinced by these models. However, the increases in uncertainty introduced by these measures also illustrate that increasing model complexity generally requires the support of increased observation.

9.2. Effective discharge of suspended sediment

The overall picture of suspended sediment discharge for the lower Salinas River is one dominated by rare, large flood events at the multi-decadal scale. Greater than half the Q_{SS} is transported by high discharges during flood events with recurrence intervals of ~3 to 7 years. In contrast, the most effective transport of water takes place at discharge magnitudes near Q_{mean}, and the majority of water is transported by flood events with return intervals of <~2 years. However, lower magnitude discharges, on the order of 10–20 Q_{mean} move a significant amount of sediment in this system, on par with that of rare, high discharge ranges (>1500 m^3/s, or ~130 Q_{mean}).

The two estimates based on LOESS temporally zoned and multiple regression rating curves each bore widely different effective discharge estimations (465 vs. 1811 m^3/s, corresponding to 40 and 156 times Q_{mean}, respectively) and $Q_{1/2}$ (498 vs. 814 m^3/s, corresponding to 42 and 72 time Q_{mean}, respectively) for Q_{SS}. Indeed, the many methods of Q_{SS} estimation employed in this study produced a wide range of magnitude/frequency estimates, although $Q_{1/2}$ for sand were generally higher than for fines and temporally stratified estimates of $Q(e)$ were generally the same or higher than for total temporal domain estimates. All of these values are much higher than the corresponding effective and half-load discharges of water, which are 9.9 and 134 m^3/s (0.9 and 11.6 times Q_{mean}) respectively. Thus, a relatively small fraction of water is transported by the moderate to very high magnitude discharges which transport most of the suspended sediment through the lower Salinas River.

This characteristic of the Salinas is similar to the transport effectiveness of suspended sediment in other highly episodic, small rivers draining the Coast Ranges of California. For example, the lower Eel River has been found to have a wide range of similar magnitude $e(Q)$ values from ~5 to 25 Q_{mean}, with a distinct $Q(e)$ peak at ~31 Q_{mean} (Klonsky and Vogel, 2011). The lower $Q(e)/Q_{mean}$ value of the Eel relative to the Salinas is most likely due to its position in the wetter north coast ranges. In contrast, larger rivers with more continuous flow characteristics generally have lower $Q(e)$ and $Q_{1/2}$ values, which are even closer to Q_{mean} and more in line with the magnitude/frequency characteristics of water in those systems (Nash, 1994).

Temporal zones of persistent sediment behavior varied in $Q(e)$ placement due to changes in sediment rating curve shape. Sand behavior displayed a consistent shift in effective discharge from the moderate discharge $e(Q)$ cluster (10–40 Q_{mean}) to extremely high discharge (170 Q_{mean}) when moving from the high C_{SS} period (1967–1986) to the low C_{SS} period (1987–2010), due to the steeper rating curve for the latter zone (see Figs. 6d, e, and 12). In contrast, fine sediment estimates based on LOESS curves resulted in very similar $Q(e)$ values for the 1991–1993 positive residual period and the joint negative residual periods (1980–1989, 1994–2011), while the positive residual period (1967–1979) resulted in a much higher $Q(e)$ due to steep curvature of the rating curve in the upper discharge domain (see Figs. 5a–c, and 11). Thus, even for a given distribution of flow probabilities, it is clear that non-stationarity in suspended sediment behavior leads to non-stationarity in effective discharge, which can cause the lower Salinas to behave more like a larger or wetter river, or like a smaller, more arid system depending on the period of activity.

9.3. The role of ENSO in suspended sediment discharge

As reported by Farnsworth and Milliman (2003), large infrequent events almost always occur during El Niño years. Magnitude/frequency analysis clearly shows that moderate to high discharges accounts for most of the sediment transported through the lower Salinas at the inter-decadal scale. Furthermore, short elapsed time since the last moderate to high discharge activity has been shown to increase sand concentrations (Gray et al., 2014a). Thus, El Niño cycles appear to increase total Q_{SS} and augment sand supply due to closer timing of these high discharge events. Indeed, temporally zoned LOESS, and multiple regression with antecedent flow indices both showed that El Niño years transported an order of magnitude more sediment on average than non-El Niño years, with similar proportional contributions of fines and sand (see Table 3). These conclusions are in broad agreement with the findings of previous studies that have highlighted the importance of El Niño on sediment transport in southern California (Inman and Jenkins, 1999; Farnsworth and Milliman, 2003; Andrews and Antweiler, 2012).

Investigation into the proportional effect of antecedent flow indices on fine C_{SS} estimations from multiple regression showed that Q_{114} *Time* was on average greater than the negative adjustment of Q_1 *Time* during 1967–1979, while the negative adjustments from Q_1 *Time* were on average larger than the positive contributions of Q_{114} *Time* from 1980–1989 (see Table 4). However, Q_{114} *Time* also beat out Q_1 *Time* during the negative fine sediment zone 1994–2011. These findings are also largely in agreement with those of a previous study on decadal scale persistence in C_{SS}–Q relationships in the Salinas River, where changes in the dominance of these indices were also implied (Gray et al., 2014b). Other long term factors operating at the watershed scale not addressed in this study, such as changes in land us practices, may be responsible in part for this apparent shift in hydrologic variable control on suspended sediment behavior.

10. Conclusions

This study produced the following results regarding lower Salinas suspended sediment behavior and flux:

- The interaction of short observed data base period and decadal scale persistence in suspended sediment behavior resulted in over estimation of Salinas River mean annual Q_{SS} by ~0.8 Mt/yr (~25%) by previous studies.
- With current data availability, sediment discharge from the Salinas River is best approximated by LOESS rating curves based on longer periods of observed data that are not limited to one period of persistent suspended sediment behavior.
- Accounting for time-dependence and/or the effects of antecedent basin conditions can inform the evaluation of estimates from single temporal domain, single independent variable rating curves, but requires more observed data to decrease estimate uncertainty.
- Most Q_{SS} through the lower Salinas occur during large (peak $Q > 40\ Q_{mean}$) rare events with return intervals >3 years, which is consistent with highly episodic, steep coastal systems on active margins, but not as extreme as observed on truly arid rivers.
- However, periods of persistent sediment behavior can shift the system toward moving a higher proportion of sediment during lower discharges, as well as shift toward emphasis on even rarer events (return interval ~20 year) due to changes in the $C_{SS} \sim Q$ relationship.
- El Niño years were responsible for ~10 times more Q_{SS} on average than non-El Niño years from 1967 to 2011.

Despite these limitations, this study represents a step toward enhancing the understanding of sediment flux estimation by accounting for the effects of non-stationarity. Better estimates of Q_{SS} in the lower Salinas were achieved by using longer sample records, while explicitly acknowledging persistent patterns in suspended sediment behavior and the effects of hydrologic preconditions calls into question the use of single rating curves, which may produce erroneously small confidence intervals.

The estimation of Q_{SS} in most systems continues to be computed from Q and C_{SS} through simple sediment rating curves based on samples representing relatively narrow ranges of basin conditions and short temporal domains. This is not surprising considering the additional data demands of more sophisticated techniques that account for temporal and additional variable dependencies. The simple fact remains that suspended sediment data is time consuming and costly to collect. However, the recognition of temporal dependency in the suspended sediment – discharge relationship violates the stationary assumptions necessary for estimations of long term sediment flux from short term observations. Temporal dependence can also calls into question the approaching of pooling long term data into a single base period to derive a single, aggregate rating relationship. Thus, estimates incorporating temporal dependency may be preferred as more accurate, despite broader estimated confidence intervals, as short and single base period estimates may be over confident. With a reduction in funding toward these sampling efforts across the United States, the possibility of achieving or maintaining the long-term records required to decipher long term sediment flux dynamics is reduced. However, shifting toward the use of techniques such as LOESS is advisable for cases where log-linearity of the C_{SS}–Q relationship is violated.

Acknowledgements

This research was funded largely by the National Science Foundation under award No. 0628385. Additional support for the lead author was provided by an Ernest E. Hill Fellowship, a William and Linda Sullivan Scholarship, and support from the Hydrologic Sciences Graduate Group at the University of California, Davis. This project was also supported by the USDA National Institute of Food and Agriculture, Hatch project number #CA-D-LAW-7034-H. Any opinions, findings and conclusions or recommendations expressed in this material are those of the authors and do not necessarily reflect the views of the National Science Foundation. We thank Peter Barnes, Sarah Greve, Duyen Ho, Olivia Oseguera, Larissa Salaki, and the Elkhorn Slough National Estuarine Research Reserve for laboratory and field assistance. This manuscript was significantly improved by many key insights and recommendations offered by a thorough review from Murray Hicks. Conversations with Rocko Brown were much appreciated by the lead author.

References

Andrews, E.D., 1980. Effective and bankfull discharge of streams in the Yampa River Basin, Colorado and Wyoming. J. Hydrol. 46, 311–330.
Andrews, E.D., Antweiler, R.C., 2012. Sediment fluxes from California Coastal Rivers: the influences of climate, geology, and topography. J. Geol. 120 (4), 349–366.
Andrews, E.D., Antweiler, R.C., Neiman, P.J., Ralph, F.M., 2004. Influence of ENSO on flood frequency along the California coast. J. Climate 17 (2), 337–348.
Chatterjee, S., Hadi, A.S., Price, B., 2000. Regression Analysis by Example. John Wiley & Sons Inc., New York, p. 359.
Cleveland, W.S., 1979. Robust locally weighted regression and smoothing scatterplots. J. Am. Stat. Assoc. 74, 829–836.
Cleveland, W.S., Devlin, S.J., 1988. Locally weighted regression: an approach to regression analysis by local fitting. J. Am. Stat. Assoc. 83 (403), 596–610.
Cohn, T.A., Delong, L.L., Gilroy, E.J., Hirsch, R.M., Wells, D.K., 1989. Estimating constituent loads. Water Resour. Res. 25 (5), 937–942.
Duan, N., 1983. Smearing estimate – a nonparametric retransformation method. J. Am. Stat. Assoc. 78 (383), 605–610.
Estrany, J., Garcia, C., Batalla, R.J., 2009. Suspended sediment transport in a small Mediterranean agricultural catchment. Earth Surf. Process. Landf. 34 (7), 929–940.
Farnsworth, K.L., Milliman, J.D., 2003. Effects of climatic and anthropogenic change on small mountainous rivers: the Salinas River example. Glob. Planet. Change 39 (1–2), 53–64.
Farnsworth, K.L., Warrick, J.A., 2007. Sources, Dispersal, and Fate of Fine Sediment Supplied to Coastal California: U.S. Geological Survey Scientific Investigations Report 2007-5254, p. 77.
Ferguson, R.I., 1986. River loads underestimated by rating curves. Water Resour. Res. 22 (1), 74–76.
Gao, P., Pasternack, G.B., Bali, K.M., Wallender, W.W., 2007. Suspended-sediment transport in an intensively cultivated watershed in southeastern California. Catena 69 (3), 239–252.
Gray, A.B., Pasternack, G.B., Watson, E.B., 2010. Hydrogen peroxide treatment effects on the particle size distribution of alluvial and marsh sediments. Holocene 20 (2), 293–301.
Gray, A.B., Warrick, J.A., Pasternack, G.B., Watson, E.B., Goñi, M.A., 2014a. Suspended sediment behavior in a coastal dry-summer subtropical catchment: effects of hydrologic preconditions. Geomorphology 214, 485–501.
Gray, A.B., Pasternack, G.B., Watson, E.B., Warrick, J.A., Goñi, M.A., 2014b. The effect of El Niño Southern Oscillation cycles on the decadal scale suspended sediment

behavior of a coastal dry-summer subtropical catchment. Earth Surf. Proc. Landf. doi: http://dx.doi.org/10.1002/esp.3627.

Guy, H.P., Norman, V.W., 1970. Field methods for measurement of fluvial sediment, chap. C2 of Applications of hydraulics (book 3): U.S. Geological Survey Techniques of Water-Resources Investigation, p. 59.

Helsel, D.R., Hirsch, R.M., 2002. Statistical methods in water resources—hydrologic analysis and interpretation: U.S. Geological Survey Techniques of Water-Resources Investigations, book 4, chap. A3, p. 510.

Hicks, D.M., Gomez, B., Trustrum, N.A., 2000. Erosion thresholds and suspended sediment yields, Waipaoa River Basin, New Zealand. Water Resour. Res. 36 (4), 1129–1142.

Hill, P.S., Nowell, A.R.M., Jumars, P.A., 1988. Flume evaluation of the relationship between suspended sediment concentration and excess boundary shear-stress. J. Geophys. Res. – Oceans 93, 12499–12509. http://dx.doi.org/10.1029/JC093iC10p12499.

Horowitz, A.J., 2003. An evaluation of sediment rating curves for estimating suspended sediment concentrations for subsequent flux calculations. Hydrol. Process. 17 (17), 3387–3409.

Interagency Committee on Water Data (IACWD), 1982, Guidelines for determining flood flow frequency, Bulletin No. 17B (revised and corrected), Hydrology Subcommittee, Washington, D. C.

Inman, D.L., Jenkins, S.A., 1999. Climate change and the episodicity of sediment flux of small California rivers. J. Geol. 107 (3), 251–270.

Kahana, R., Ziv, B., Enzel, Y., Dayan, U., 2002. Synoptic climatology of major floods in the Negev Desert, Israel. Int. J. Climatol. 22 (7), 867–882.

Kelsey, H.M., 1980. A sediment budget and an analysis of geomorphic process in the Van Duzen River basin, north coastal California, 1941–1975. Geol. Soc. Am. Bull. 91 (4 pt. 2), 1119–1216.

Klein, R.D., Anderson, J.K., 2012. Declining sediment loads from Redwood Creek and the Klamath River, north coastal California. In: Proceedings of the Coastal Redwood Forests in a Changing California: A Symposium for Scientists and Managers, U.S. Department of Agriculture, Forest Service General Technical Report PSW-GTR-238, pp. 79–88.

Klonsky, L., Vogel, R.M., 2011. Effective measures of "effective" discharge. J. Geol. 119 (1), 1–14.

Lopez-Tarazon, J.A., Batalla, R.J., Vericat, D., Francke, T., 2012. The sediment budget of a highly dynamic mesoscale catchment: the River Isabena. Geomorphology 138 (1), 15–28.

Milliman, J.D., Syvitski, J.P.M., 1992. Geomorphic/tectonic control of sediment discharge to the ocean: the importance of small mountainous rivers. J. Geol. 100 (5), 525–544.

Montgomery, D.C., Peck, E.A., 1992. Introduction to Linear Regression Analysis. John Wiley & Sons Inc., New York, p. 527.

Nash, D.B., 1994. Effective sediment-transporting discharge from magnitude-frequency analysis. J. Geol. 102 (1), 79–95.

Pasternack, G.B., Brush, G.S., Hilgartner, W.B., 2001. Impact of historic land-use change on sediment delivery to a Chesapeake Bay subestuarine delta. Earth Surf. Process. Landf. 26 (4), 409–427.

Pedatella, N.M., Forbes, J.M., 2009. Interannual variability in the longitudinal structure of the low-latitude ionosphere due to the El Nino-Southern oscillation. J. Geophys. Res.-Space Phys., 114.

Pelletier, J.D., Turcotte, D.L., 1997. Long-range persistence in climatological and hydrological time series: analysis, modeling and application to drought hazard assessment. J. Hydrol. 203 (1–4), 198–208.

Potter, W.D., 1958. Upper and lower frequency curves for peak rates of runoff. Trans. Amer. Geophys. Union 39, 100–105.

R Development Core Team, 2013. R: A language and environment for statistical computing. R Foundation for Statistical Computing, Vienna, Austria. <http://www.R-project.org/> (accessed 10. 13).

Rasmussen, P.P., Gray, J.R., Glysson, G.D., Ziegler, A.C., 2009. Guidelines and procedures for computing time-series suspended-sediment concentrations and loads from in-stream turbidity-sensor and streamflow data: U.S. Geological Survey Techniques and Methods book 3, chap. C4, p. 53. <http://pubs.usgs.gov/tm/tm3c4/> (accessed 3.13.13).

Rouse, H., 1937. Modern conceptions of the mechanics of fluid turbulence. Trans. Am. Soc. Civ. Eng. 102, 463–541.

Shakesby, R.S., Doerr, S.H., 2006. Wildfire as a hydrological and geomorphological agent. Earth-Sci. Rev. 74, 269–307.

Tanji, K., Singer, M., Biggar, J., Whittig, L., Henderson, D., 1980. Nonpoint sediment production in the Colusa Basin drainage area. October 1978 – September 1979. Second-year annual progress report on EPA Grant No. R805462. University of California, Davis, Water Science and Engineering Paper No. 4018, 379p.

U.S. Geological Survey National Water Information System (USGS NWIS), <http://waterdata.usgs.gov/nwis/sw> (accessed 03.13).

U.S. Army Corps of Engineers (USACE), 2010. HEC-SSP, Statistical Software Package, User's Manual, Version 2.0, CPD-86, Institute for Water Resources, Davis, CA, USA.

Vogel, R.M., Stedinger, J.R., Hooper, R.P., 2003. Discharge indices for water quality loads. Water Resour. Res. 39 (10).

Walling, D.E., 1977. Assessing the accuracy of suspended sediment rating curves for a small basin. Water Resour. Res. 13 (3), 531–538.

Wand, M.P., 2012. KernSmooth: Functions for kernel smoothing for Wand & Jones (1995). R package version 2.23-8. <http://CRAN.R-project.org/package=KernSmooth> (accessed 3.13.13).

Wand, M.P., Jones, M.C., 1995. Kernel Smoothing. Chapman and Hall, London, p. 212.

Warrick, J.A., Mertes, L.A.K., 2009. Sediment yield from the tectonically active semiarid Western Transverse Ranges of California: Geological Society of America. Bulletin 121, 1054–1070.

Warrick, J.A., Rubin, D.M., 2007. Suspended-sediment rating curve response to urbanization and wildfire, Santa Ana River, California. J. Geophys. Res. – Earth Surf. 112 (F2).

Warrick, J.A., Hatten, J.A., Pasternack, G.B., Gray, A.B., Goni, M.A., Wheatcroft, R.A., 2012. The effects of wildfire on the sediment yield of a coastal California watershed. Geol. Soc. Am. Bull. 124 (7–8), 1130–1146.

Warrick, J.A., Madej, M.A., Goni, M.A., Wheatcroft, R.A., 2013. Trends in the suspended-sediment yields of coastal rivers of northern California, 1955–2010. J. Hydrol. 489, 108–123.

Wass, P.D., Leeks, G.J.L., 1999. Suspended sediment fluxes in the Humber catchment, UK. Hydrol. Process. 13, 935–953. http://dx.doi.org/10.1002/(SICI)1099-1085(199905)13:7<935::AID-HYP783>3.0.CO;2-L.

Webb, B.W., Walling, D.E., 1982. The magnitude and frequency characteristics of fluvial transport in a Devon drainage basin and some geomorphic implications. Catena 9, 9–23.

Wheatcroft, R.A., Goni, M.A., Hatten, J.A., Pasternack, G.B., Warrick, J.A., 2010. The role of effective discharge in the ocean delivery of particulate organic carbon by small, mountainous river systems. Limnol. Oceanography 55 (1), 161–171.

Williams, G.P., 1989. Sediment concentration versus water discharge during single hydrologic events in rivers. J. Hydrol. 111 (1–4), 89–106.

Wolman, M.G., Miller, J.P., 1960. Magnitude and frequency of forces in geomorphic processes. J. Geol. 68 (1), 54–74.

Wolman, M.G., Shick, A.P., 1967. Effects of construction on fluvial sediment; urban and suburban areas of Maryland. Water Resour. Res. 3, 451–464.

Wolter, K., Timlin, M.S., 2011. El nino/southern oscillation behaviour since 1871 as diagnosed in an extended multivariate ENSO index (MEI.ext). Int. J. Climatol. 31 (7), 1074–1087.

Yu, B., 2000. A systematic over-estimation of flows. J. Hydrol. 233 (1–4), 258–262.